Doctoral Dissertation (Shinshu University)

Electromagnetic interference shielding anisotropy of CFRP composites and its applications

CFRP 複合材料の電磁波遮蔽異方性とその応用に関する研究

September 2021

Hong Jun

Abstract

Carbon fiber-reinforced composite materials have excellent mechanical properties and electromagnetic interference (EMI) shielding performance. Recently, their EMI shielding performance has also attracted great attention in many industrial fields to resolve electromagnetic pollution. Carbon fiber reinforced polymers (CFRP) composites, particularly prepreg stacked composites, have anisotropic properties, including anisotropy of electrical conductivity and dielectric characteristics. These features lead to EMI shielding anisotropy of the CFRP. Besides, when CFRP is damaged internally, its EMI shielding performance will be significantly affected, making it possible to use EM microwave technology for non-destructive testing of CFRP. This study mainly focused on investigating EMI shielding anisotropy and shielding mechanisms of CFRP composites. Theoretical formulas were proposed to analyze and predict the electrical conductivity and EMI shielding performance of CFRP composites. Moreover, the application of the EM microwave technique to the non-destructive testing (NDT) of CFRP composites were also discussed. The significant results obtained from this research are as follow:

(1) The coaxial transmission line method was used to test the EMI shielding performance of CFRP to clarify the EMI shielding anisotropy of CFRP. Moreover, the optimization of EMI shielding performance of CFRP by changing the composites' structure were also discussed. The anisotropy of EMI shielding was confirmed for the

first time by the coaxial transmission line method. A quasi-radial sample had the highest shielding effectiveness (25.8 dB) at 15 GHz, and the carbon fibers in this sample aligned in the direction of the electric field of electromagnetic waves. A CFRP composite with fibers in a parallel (0°/0°) arrangement had the lowest SE (15.9 dB) at the same frequency. Hence, the orientation of fibers relative to the direction of electric field clearly affected the EMI shielding performance of the CFRP composites. The four-ply CFRP (0°/90°/0°/90°) with three cross-layers had the highest shielding value of 28.9 dB at 15 GHz, that was far superior to that of a unidirectional CFRP (0°/0°/0°/0°) composite (SE= 18.6 dB), and it even outperformed an eight-ply unidirectional CFRP composite (SE= 22.6 dB). Cross-layering the fibers improved SE, and the number of cross-layers in the composites governed their EMI shielding performance. These findings demonstrate that optimizing the fiber orientation in CFRP composites can be a cost-effective way to achieve highly efficient EMI shielding.

(2) The electrical conductivity of unidirectional CFRP composites was identified to vary with the fiber orientation angles, and formula was used to predict the results consistent with the experimental. The obvious EMI shielding anisotropy of unidirectional CFRP composites was clarified by free-space measurement. A comparison of free-space measurement and coaxial transmission line method was also conducted, and the influence of electric anisotropy on the test results was further discussed, which indicated that special attention should be paid to the influence of the anisotropy of CFRP composites on the shielding results. With those results, the mechanism of EMI shielding anisotropy of CFRP composites is clarified, which will

provide an effective design of EMI shielding products with a designable shielding direction and frequency.

(3) The application of the electromagnetic (EM) wave technique to the non-destructive test of CFRP has been discussed. A new type of NDT method using electromagnetic wave technique (EMW-NDT) was proposed. The results present that the EM wave testing method has good detection sensitivity to the delamination size and thickness inside the CFRP composites. A reasonable sensitivity to the damage volume change in delamination was confirmed with a damage area ratio of 12.6%/dB and a thickness change of 5.5 dB/mm. It was found that the incident angle of the EM wave plays a vital role in detecting sensitivity because of the skin effect in CFRP composites. In terms of crack damage, the slit and its length were detected and the slit direction was successfully identified in this study based on the characteristics of the EMI shielding anisotropy in CFRPs.

CONTENTS

Chapter 1

General introduction

1 General introduction

1.1 Introduction

Nowadays, with the development of electronic technology and the invention of new communication equipment, more and more electrical and electronic devices appear in daily life. While this brings convenience to people's lives, the accompanying electromagnetic pollution has also become a severe problem. Electromagnetic radiation emitted by the electric devices especially operated at the microwave range of frequencies can cause malfunction of electronics [1]. Even in hospitals, mobile phones have become a potential source of interference to medical equipment, increasing the potential risk of medical accidents [2, 3]. Besides, when the human body is exposed to electromagnetic radiation for a long time, it will affect human health, such as heart disease and other diseases [4-6]. Therefore, the development of effective and applicable electromagnetic interference (EMI) shielding materials in various fields has received extensive attention in the past few decades.

Different application fields have additional performance requirements for electromagnetic shielding materials, such as precision electronic equipment, antenna equipment, and medical equipment. Generally, electrical conductivity improves the electromagnetic shielding performance of materials. EMI shielding materials with high conductivity are to reflect electromagnetic waves into the space environment, which is

likely to cause secondary pollution of electromagnetic radiation. Therefore, some application fields have significant requirements for the absorbing performance of shielding materials. Carbon materials and its composites have attracted a lot of attention for used as EMI shielding materials because of their superior mechanical properties, electromagnetic properties, and processability. Particularly, conventional carbon fiber-reinforced composite materials have excellent electrical and mechanical properties as a structure composites, which can meet the EMI shielding performance and mechanical properties' requirements. Simultaneously, changes in carbon fiber-reinforced composite materials' structure can lead to changes in its EMI shielding performance, such as fiber fracture and delamination. Therefore, the non-destructive testing of CFRP through changes in EMI shielding performance becomes possible.

1.2 Mechanisms of EMI shielding

When electromagnetic (EM) waves are incident on the shielding material's surface, part of it will be reflected. This part of the electromagnetic loss is called reflection loss. The reflection mechanism requires that the shielding material obtaining a charge carrier. Naturally, the shielding material impedance is quite different from the space impedance, and this impedance mismatch will promote the reflection of EM waves [7, 8]. Furthermore, the EM waves could interact with the magnetic and electric dipoles in the shield, which needs the shielding materials to obtain good permeability and permittivity. Finally, the EM wave could be conducted to other energies such as heat. This shielding mechanism is called absorption loss. Meanwhile, the third shielding mechanism of

multiple reflections could have happened when the shield has a large interface or surface. But the multiple reflection would be regardless when the absorption effectiveness is higher than 15 dB, and the thickness of the shield is greater than the skin depth [9, 10].

Shields with reflection as the primary mechanism will reflect incident electromagnetic waves into the environment, causing secondary EM pollution and interference with nearby electronic products. Therefore, many applications have high requirements on the absorbing properties of shielding materials. Generally, when designing such materials, the impedance mismatch between the shielding material and the free space should be minimized so that EM waves are not reflected and enter the shielding material. Simultaneously, the electric and magnetic dipoles inside the material should be increased during the design process to sufficiently absorb the incident electromagnetic waves.

1.3 EMI shielding materials

1.3.1 Metal materials

EMI shielding materials have been developed for decades. The most common shielding materials are metal materials, including aluminum, copper, iron materials, etc. They have been used as EMI shielding materials in various forms. Sheet metal is a common material used for the electronic enclosure products. It has good mechanical properties and EMI shielding performance, and the primary shielding mechanism is

reflection. However, metal materials have disadvantages such as heavyweight, inability to resist corrosion, and inflexibility, limiting their application fields. Some studies have used metal particles, fibers, and other forms to reinforce polymers and fabricated EMI shielding composite materials. Although it overcomes many shortcomings of metal materials, but it also brings defects such as poor mechanical properties and low high-temperature resistance. Metallic coating [11-13] has been used to enhance the shielding performance of shielding materials, and its common preparation methods including spraying [14, 15], electroplated coating [16, 17] and electroless coating [18, 19]. These metallic coating methods can improve materials' conductivity and further enhance the EMI shielding performance, but still have disadvantages such as weak wear performance and low environmental tolerance.

1.3.2 Carbon materials for EMI shielding

Carbon materials（such as carbon nanotube, graphene, graphite, and carbon fibers ）are possessing excellent electrical properties (electrical conductivity, permittivity, and permeability). Consequently, those carbon materials and their composites can provide superior EMI shielding performance [20-25].

1.3.2.1 Carbon-based nanomaterials

Carbon nanotubes (CNT) has been used for the efficient EMI shielding materials due to its excellent mechanical property, outstanding electrical performance and good shielding performance [26-29]. It can be synthesized by several techniques [30-33]. CNT reinforced polymer composite is a relatively common material used for

electromagnetic shielding. Zeng et al [34] found that the PVDF/CNTs/Ni@ CNTs composite films exhibit the efficient SE/thickness(d) of 102.8 dB mm^{-1}, and the EMI shielding performance was improved after the heat treatment process. Mei et al [35] presented a 3D CNT sponges with variable compaction ratios shows excellent EMI shielding performance, and the sponge had the excellent electrical conductivity and EMI shielding when the compaction ratios reached to 70%. Besides, our preview works [36-38] also proved the outstanding EM absorption properties of CNT/polymers composites.

Graphene is another carbon nanomaterial studied for EMI shielding. It has demonstrated excellent electrical conductivity, outstanding corrosion resistance, and good mechanical properties. Graphene and its composites have shown excellent EMI shielding properties, especially its EM absorption performance [39-42]. Wan et al. [23] have fabricated large-sized graphene sheets with exceptional EMI shielding properties, and found that the iodine doping can further improve the shielding performance of graphene sheets up to 52.2dB. Fan et al. [43] developed a lightweight MXene/graphene hybrid foam by freeze-drying and reduction heat treatment, and the excellent electrical conductivity and highly efficient wave attenuation of the foams reach to an excellent EMI shielding effectiveness of 50.7 dB. Liang et al. [44] fabricated highly aligned reduced graphene oxide films/epoxy composites which shows excellent EMI shielding effectiveness (82dB). In addition, graphene aerogels [45, 46] and graphene coated materials [47] also show superior EMI shielding property. Although carbon material has been studied as high-performance shielding materials, it still faces the problem of

dispersion, and its reinforced polymer composites are not resistant to high temperatures.

1.3.2.2 Graphite and carbon black

Graphite [48-50] and carbon black [51, 52] are always used as reinforcement to fabricate conductive polymer composites due to their good electrical conductivity. And they also have been used for EMI shielding materials due to their excellent electrical conductivity. Parveen Saini et al. [53] used different weight ratios of aniline to graphite to prepare polyaniline–graphite composites via in situ emulsion pathway. The shield material shows good electrical conductivity and thermal stability and exhibited excellent EMI shielding performance. Sykam et al. [54] fabricated a lightweight, flexible graphite sheet by using exfoliated graphite, which shows an excellent EMI shielding effectiveness up to 79.4 dB at a frequency of 12 GHz for 0.5 mm thickness. Other research works also show good EMI shielding performance of carbon black reinforced composites [55, 56], but its electrical conductivity and EMI shielding were lower than MWCNT and CNT based nanocomposites [57].

1.3.2.3 Carbon fibers

Carbon fiber has become a popular EMI shielding material for its good mechanical properties, lightweight and electrical conductivity [58-60]. The continuous carbon fiber composite material [61, 62] can be used as a structural composite material, and its excellent electrical properties can be used as a protective shell for precision instruments. Zhao et al. [63] found that the overlap angle and array spacing can influence the EMI shielding of carbon fiber composites, and the EMI shielding effectiveness could be reached to 60.49 dB for the array spacing of 12mm at a suitable overlap angle. Jou et

al. [64] investigated the effect of weave type, angle of overlapped palates on the EMI shield performance of continuous carbon fiber composites, and the result shows that the triple-overlapped, plain-weave composites exhibited the highest EMI shielding values of more than 100 dB at 0.9 GHz. In addition, there are also other research works reports that the EMI shielding performance of carbon fiber reinforced composites could be improved by using modified carbon fibers or adding conductive materials in it [65-69]. Unfortunately, all researchers have focused on improving the material's EMI shielding performance by modifying and adjusting the composite material structure but ignored the EMI shielding anisotropy of carbon fiber-reinforced composite materials.

1.4 EMI shielding measurements

Generally, there are four methods used to evaluate EMI shielding property: Transmission line method, shielded box method, shield room method and free-space method [70]. The transmission line method is currently the most widely used electromagnetic shielding test method. The test sample is fabricated into annular form with a specific outer and inner diameter according to ASTM D4935. By this method, the reflection, absorption and transmitted components of total shielding can be obtained separately. The electrical contact between sample and testing fixture directly affects the test result of EMI shielding, which has been proved by Asma A. Eddib [71]. Coaxial transmission line method is currently recognized as a standard method for the measurement of planner shield [72]. Shield box measurement consist of a metal box and an electrically tight seam with a sample port [73], a good electrical contact between

sample and box is the key for an accurate result but it seemed difficult to achieve it from some research report. In addition, the range of frequency should be limited within 500MHz [70]. The development of EMI shielding room method can further avoid the interference of external EM waves. It also overcomes the drawbacks within the shield box method, the frequency range for shielding test is enlarged and the reproducibility of the result has been improved. Free-space method is defined as open field method, the test setup is made up of two horn antennas, network analyzer and sample holder. The advantage of free space measurement is allowing the measurement conducted without any physical contact with the sample, compared to the transmission line technique, for which the sample is deformed into a particular shape, depending on the transmission line used, either waveguide or coaxial type [74].

1.5 Non-destructive testing of Carbon fiber reinforced composites

There are currently many NDT methods to detect defects and damages within composite materials. Among them, the eddy current testing method has been attracted much attentions and been extensively studied. The eddy current testing method is a non-contact method that is mainly used to detect cracks and corrosions within materials with high conductivity [75, 76]. In order to improve the detection effect in CRRP, Wu et al. developed a T-R probe with a special structure to overcome the impact of lift-off variation and obtained high sensitivity to defects within CFRP [77]. Mizukami et al. designed and changed the probe geometry of eddy current testing setup to improve the

sensitivity to delamination of CFRP, and the delamination with a length and width of 10mm could be observed [78]. He et al. found that the defects induced by low-energy impact can be effectively defected by scanning pulsed eddy current testing [79]. Many researchers also study the application of Eddy current testing in CFRP detection through modeling [80, 81]. Due to the eddy current test method's electrical performance requirements, the test used for CFRP testing is not mature. At the same time, eddy current also has many disadvantages, such as the limitation of penetration depth and not suitable for the detection of complex geometries and large area materials.

Another prevalent and widely used NDT method is the ultrasonic testing, which has mainly been used to detect material delamination. The pulse-echo method is often applied to thickness measurements and flaw location, and the ultrasonic C-scan technique can show the location, orientation, and size of defects. Several research show it can be applied to the detection of impact damage in CFRP [82-84]. However, there are still many disadvantages that apply the ultrasonic testing to detect CFRP materials. For example, a medium is required to transmit ultrasonic energy from the probe to the composite material, such as water and gel, and it isn't easy to detect the delamination that existed near the surface of materials [78, 85]. Although some researchers have developed ultrasonic detection methods that do not require couple medium, the test has many limitations and must be performed under specific conditions [86, 87]. Moreover, some irregularly shaped materials or materials with rough surfaces are difficult to test and get accurate results.

EM wave method such as free-space measurement is a non-contact and non-

destructive measurement, and the couple medium is not needed for the test. It can test samples of large size and various shapes, so it will not damage the material during the trial. Free-space measurement is usually used to determine the magnetic permeability and electric permittivity of materials that even could be conducted under different temperature conditions [88, 89]. Some research work shows the possibility of applying a free-space non-destructive method to detect hardened cement specimens [90] and determine the dispersion and orientation of fiber that existed in concretes [91]. However, few reports are on the application of the free-space measurement to the non-destructive testing of CFRP, especially the evaluation of the CFRP's delamination.

1.6 Purposes and significances of research

The purpose of this study is to investigate the EMI shielding anisotropy and shielding mechanisms of CFRP composites. We try to identify the EMI shielding mechanisms of CFRP composite and predict its shielding performance by proposed theoretical formulas. Besides, we also want to confirm the feasibility of EM microwave technology in applying non-destructive testing of CFRP. First, the coaxial transmission line method was used to test CFRP composites to clarify its EMI shielding anisotropy. We investigated the factors that affect the shielding ability of CFRP composites, such as the fiber orientation, thickness and fiber types. Moreover, the optimization of EMI shielding performance of CFRP by changing the composites' structure were also discussed.

To further investigated the EMI shielding anisotropy of CFRP composites, we

applied a specified set-up of free-space measurement to test it. EMI shielding anisotropy of unidirectional CFRP composites was discussed, and the theoretical formula was used to predict EMI SE of CFRP at various carbon fiber orientations. Meanwhile, a comparison of free-space measurement and coaxial transmission line method was also conducted, and the influence of EMI shielding anisotropy on the test results with different measurements was discussed.

In addition, damage such as fiber breakage and delamination is likely to occur inside the material when subjected to external forces, like impact and fatigue load. Those damages are mostly invisible and can bring safety hazards during the service of the product. This study aimed to propose a new type of NDT method using electromagnetic wave (EMW-NDT) to detect the damage in CFRP composites. The inspection ability of this method in relation to the different types of damages inside CFRP composites is investigated. The detection capacity of the EMW-NDT method to the delamination size, thickness, and crack of CFRP were also discussed.

1.7 Outline of dissertation

This dissertation is organized to summarize electromagnetic interference shielding anisotropy of CFRP composites and its applications.

In Chapter 1, an overview of the EMI shielding materials, shielding mechanisms, EMI shielding measurements, and the NDT testing of CFRP has been present.

In Chapter 2, the anisotropy of EMI shielding was confirmed for the first time by the coaxial transmission line method, and the optimization of EMI shielding

performance of CFRP by changing the composites' structure was studied. Meanwhile, the shielding mechanisms of CFRP with various fiber orientation were also discussed.

In Chapter 3, the obvious EMI shielding anisotropy of unidirectional CFRP composites was clarified by a specified set-up of free-space measurement. The theoretical formulas were used to predicted the electrical conductivity and EMI shielding effectiveness of CFRP, respectively.

In Chapter 4, based on the electromagnetic wave technique, a new type of NDT method using electromagnetic wave (EMW-NDT) was proposed to predict the damages of CFRP composites. The detect sensitivity of NDT method to the damages were also discussed.

In Chapter 5, a summary of the research and conclusions were presented.

References

[1] D.D.L. Chung, Materials for electromagnetic interference shielding, Materials Chemistry and Physics 255 (2020) 123587.

[2] E. Hanada, K. Kodama, K. Takano, Y. Watanabe, Y. Nose, Possible Electromagnetic Interference with Electronic Medical Equipment by Radio Waves Coming from Outside the Hospital, Journal of Medical Systems 25(4) (2001) 257-267.

[3] G. Calcagnini, F. Censi, M. Floris, C. Pignalberi, R. Ricci, G. Biancalana, Evaluation of Electromagnetic Interference of GSM Mobile Phones with Pacemakers Featuring Remote Monitoring Functions, Electromagnetic interference to pacemaker 29 (2006) 380-385.

[4] J. Grellier, P. Ravazzani, E. Cardis, Potential health impacts of residential exposures to extremely low frequency magnetic fields in Europe, Environ Int 62 (2014) 55-63.

[5] S. Gupta, N.-H. Tai, Carbon materials and their composites for electromagnetic interference shielding effectiveness in X-band, Carbon 152 (2019) 159-187.

[6] J. Schuz, A. Ahlbom, Exposure to electromagnetic fields and the risk of childhood leukaemia: a review, Radiat Prot Dosimetry 132(2) (2008) 202-11.

[7] M.-S. Cao, W.-L. Song, Z.-L. Hou, B. Wen, J. Yuan, The effects of temperature and frequency on the dielectric properties, electromagnetic interference shielding and microwave-absorption of short carbon fiber/silica composites, Carbon 48(3) (2010) 788-796.

[8] H. Saadi, R. Oussaid, Materials effect on shielding effectiveness, IEEE International Conference on Signal Processing and Communications (ICSPC 2007),, IEEE, Dubai, United Arab Emirates, 2007.

[9] J. Joo, A.J. Epstein, Electromagnetic Radiation Shielding by Intrinsically Conducting Polymers, Applied Physics Letters 65(18) (1994) 2278-2280.

[10] N.C. Dasa, D. Khastgira, T.K. Chakia, A. Chakrabortyb, Electromagnetic interference shielding effectiveness of carbon black and carbon fibre filled EVA and NR based composites, Composites: Part A 31 (2000) 1069-1081.

[11] J.T. Hoback, J.J. Reilly, Conductive Coatings for EMI Shielding, Journal of

elastomers and plastics 20 (1988) 54-69.

[12] A. Das, H.T. Hayvaci, M.K. Tiwari, I.S. Bayer, D. Erricolo, C.M. Megaridis, Superhydrophobic and conductive carbon nanofiber/PTFE composite coatings for EMI shielding, J Colloid Interface Sci 353(1) (2011) 311-5.

[13] Y.K. Hong, C.Y. Lee, C.K. Jeong, J. Joo, Electromagnetic interference shielding characteristics of fabric complexes coated with conductive polypyrrole and thermally evaporated Ag, Current Applied Physics 1(6) (2001) 439-442.

[14] Y. Li, H. Zhang, Y. Liu, H. Wang, Z. Huang, T. Peijs, E. Bilotti, Synergistic effects of spray-coated hybrid carbon nanoparticles for enhanced electrical and thermal surface conductivity of CFRP laminates, Composites Part A: Applied Science and Manufacturing 105 (2018) 9-18.

[15] Q. Wen, W. Zhou, J. Su, Y. Qing, F. Luo, D. Zhu, High performance electromagnetic interference shielding of lamellar $MoSi_2$/glass composite coatings by plasma spraying, Journal of Alloys and Compounds 666 (2016) 359-365.

[16] X. Shui, D.D.L. Chung, Submicron nickel filaments made by electroplating carbon filaments as a new filler material for electromagnetic interference shielding, Journal of Electronic Materials 24 (1995) 107-113.

[17] H. Guo, Z.-q. Chen, J.-j. Li, L. Li, Study of Fe/Ni alloy coated carbon fibres prepared by electroplating, Surface Engineering 35(10) (2018) 841-847.

[18] E.G. Han, E.A. Kim, K.W. Oh, Electromagnetic interference shielding effectiveness of electroless Cu-plated PET fabrics, Synthetic Metals 123 (2001) 469-476.

[19] Y. Lu, S. Jiang, Y. Huang, Ultrasonic-assisted electroless deposition of Ag on PET fabric with low silver content for EMI shielding, Surface and Coatings Technology 204(16-17) (2010) 2829-2833.

[20] M.H. Al-Saleh, U. Sundararaj, Electromagnetic interference shielding mechanisms of CNT/polymer composites, Carbon 47(7) (2009) 1738-1746.

[21] I.W. Nam, H.K. Lee, J.H. Jang, Electromagnetic interference shielding/absorbing characteristics of CNT-embedded epoxy composites, Composites Part A: Applied

Science and Manufacturing 42(9) (2011) 1110-1118.

[22] J. Liang, Y. Wang, Y. Huang, Y. Ma, Z. Liu, J. Cai, C. Zhang, H. Gao, Y. Chen, Electromagnetic interference shielding of graphene/epoxy composites, Carbon 47(3) (2009) 922-925.

[23] Y.-J. Wan, P.-L. Zhu, S.-H. Yu, R. Sun, C.-P. Wong, W.-H. Liao, Graphene paper for exceptional EMI shielding performance using large-sized graphene oxide sheets and doping strategy, Carbon 122 (2017) 74-81.

[24] Y. Liu, K. Zhang, Y. Mo, L. Zhu, B. Yu, F. Chen, Q. Fu, Hydrated aramid nanofiber network enhanced flexible expanded graphite films towards high EMI shielding and thermal properties, Composites Science and Technology 168 (2018) 28-37.

[25] A. Ameli, P.U. Jung, C.B. Park, Electrical properties and electromagnetic interference shielding effectiveness of polypropylene/carbon fiber composite foams, Carbon 60 (2013) 379-391.

[26] N. Li, Y. Huang, F. Du, Y. Chen, P. C.Eklund, Electromagnetic Interference (EMI) Shielding of Single-Walled Carbon Nanotube Epoxy Composites, Nano Letters 6(6) (2006) 1141-1145.

[27] E.G. Barathi Dassan, A. Anjang Ab Rahman, M.S.Z. Abidin, H.M. Akil, Carbon nanotube–reinforced polymer composite for electromagnetic interference application: A review, Nanotechnology Reviews 9(1) (2020) 768-788.

[28] Q. Song, F. Ye, X. Yin, W. Li, H. Li, Y. Liu, K. Li, K. Xie, X. Li, Q. Fu, L. Cheng, L. Zhang, B. Wei, Carbon nanotube-multilayered graphene edge plane core-shell hybrid foams for ultrahigh-performance electromagnetic-interference shielding, Adv Mater 29(31) (2017).

[29] Y.-D. Shi, J. Li, Y.-J. Tan, Y.-F. Chen, M. Wang, Percolation behavior of electromagnetic interference shielding in polymer/multi-walled carbon nanotube nanocomposites, Composites Science and Technology 170 (2019) 70-76.

[30] N. Braidy, M.A.E. Khakani, G.A. Botton, Effect of laser intensity on yield and physical characteristics of single wall carbon nanotubes produced by the Nd:YAG laser vaporization method, Carbon 40 (2002) 2835-2842.

[31] C.T. Kingston, B. Simard, Fabrication of Carbon Nanotubes, Analytical Letters 36(15) (2003) 3119-3145.

[32] N.H. Tai, H.M. Chen, Y.J. Chen, P.Y. Hsieh, J.R. Liang, T.W. Chou, Optimization of processing parameters of the chemical vapor deposition process for synthesizing high-quality single-walled carbon nanotube fluff and roving, Composites Science and Technology 72(15) (2012) 1855-1862.

[33] D. Zhou, E.V. Anoshkina, L. Chow, G. Chai, Synthesis of carbon nanotubes by electrochemical deposition at room temperature, Carbon 44(5) (2006) 1013-1016.

[34] S. Zeng, X. Li, M. Li, J. Zheng, S. E, W. Yang, B. Zhao, X. Guo, R. Zhang, Flexible PVDF/CNTs/Ni@CNTs composite films possessing excellent electromagnetic interference shielding and mechanical properties under heat treatment, Carbon 155 (2019) 34-43.

[35] H. Mei, X. Zhao, J. Xia, F. Wei, D. Han, S. Xiao, L. Cheng, Compacting CNT sponge to achieve larger electromagnetic interference shielding performance, Materials & Design 144 (2018) 323-330.

[36] Y.F. Zhu, L. Zhang, T. Natsuki, Y.Q. Fu, Q.Q. Ni, Facile synthesis of BaTiO3 nanotubes and their microwave absorption properties, ACS Appl Mater Interfaces 4(4) (2012) 2101-6.

[37] Y.-F. Zhu, Q.-Q. Ni, Y.-Q. Fu, One-dimensional barium titanate coated multi-walled carbon nanotube heterostructures: synthesis and electromagnetic absorption properties, RSC Advances 5(5) (2015) 3748-3756.

[38] Y.-F. Zhu, Y.-Q. Fu, T. Natsuki, Q.-Q. Ni, Fabrication and microwave absorption properties of BaTiO3 nanotube/polyaniline hybrid nanomaterials, Polymer Composites 34(2) (2013) 265-273.

[39] M. Cao, C. Han, X. Wang, M. Zhang, Y. Zhang, J. Shu, H. Yang, X. Fang, J. Yuan, Graphene nanohybrids: excellent electromagnetic properties for the absorbing and shielding of electromagnetic waves, Journal of Materials Chemistry C 6(17) (2018) 4586-4602.

[40] A. Joshi, A. Bajaj, R. Singh, A. Anand, P.S. Alegaonkar, S. Datar, Processing of

graphene nanoribbon based hybrid composite for electromagnetic shielding, Composites Part B: Engineering 69 (2015) 472-477.

[41] K. Sabira, M.P. Jayakrishnan, P. Saheeda, S. Jayalekshmi, On the absorption dominated EMI shielding effects in free standing and flexible films of poly(vinylidene fluoride)/graphene nanocomposite, European Polymer Journal 99 (2018) 437-444.

[42] Q. Jiang, X. Liao, J. Li, J. Chen, G. Wang, J. Yi, Q. Yang, G. Li, Flexible thermoplastic polyurethane/reduced graphene oxide composite foams for electromagnetic interference shielding with high absorption characteristic, Composites Part A: Applied Science and Manufacturing 123 (2019) 310-319.

[43] Z. Fan, D. Wang, Y. Yuan, Y. Wang, Z. Cheng, Y. Liu, Z. Xie, A lightweight and conductive MXene/graphene hybrid foam for superior electromagnetic interference shielding, Chemical Engineering Journal 381 (2020) 122696.

[44] C. Liang, P. Song, H. Qiu, Y. Huangfu, Y. Lu, L. Wang, J. Kong, J. Gu, Superior electromagnetic interference shielding performances of epoxy composites by introducing highly aligned reduced graphene oxide films, Composites Part A: Applied Science and Manufacturing 124 (2019) 105512.

[45] Y.-J. Wan, P.-L. Zhu, S.-H. Yu, R. Sun, C.-P. Wong, W.-H. Liao, Ultralight, super-elastic and volume-preserving cellulose fiber/graphene aerogel for high-performance electromagnetic interference shielding, Carbon 115 (2017) 629-639.

[46] Z. Wang, R. Wei, J. Gu, H. Liu, C. Liu, C. Luo, J. Kong, Q. Shao, N. Wang, Z. Guo, X. Liu, Ultralight, highly compressible and fire-retardant graphene aerogel with self-adjustable electromagnetic wave absorption, Carbon 139 (2018) 1126-1135.

[47] B. Shen, Y. Li, W. Zhai, W. Zheng, Compressible Graphene-Coated Polymer Foams with Ultralow Density for Adjustable Electromagnetic Interference (EMI) Shielding, ACS Appl Mater Interfaces 8(12) (2016) 8050-7.

[48] A. Celzard, E. McRae, J.F. Mareche, G. Furdin, Conduction mechanisms in some graphite–polymer composites: Effects of temperature and hydrostatic pressure, Journal of Applied Physics 83 (1998) 1410-1419.

[49] I. Krupa, I. Novak, I. Chodak, Electrically and thermally conductive

polyethylene/graphite composites and their mechanical properties, Synthetic Metals 145(2-3) (2004) 245-252.

[50] V. Panwar, J.-O. Park, S.-H. Park, S. Kumar, R.M. Mehra, Electrical, dielectric, and electromagnetic shielding properties of polypropylene-graphite composites, Journal of Applied Polymer Science 115(3) (2010) 1306-1314.

[51] I. Chodak, I. Krupa, "Percolation effect" and mechanical behavior of carbon black filled polyethylene, Journal of Materials Science Letters 18 (1999) 1457-1459.

[52] G. Yang, R. Teng, P. Xiao, Electrical Properties of Crosslinked Polyethylene/Carbon Black Switching Composites as a Function of Morphology and Structure of the Carbon, Polymer Composites 18 (1997) 477-483.

[53] P. Saini, V. Choudhary, K.N. Sood, S.K. Dhawan, Electromagnetic interference shielding behavior of polyaniline/graphite composites prepared by insituemulsion pathway, Journal of Applied Polymer Science 113(5) (2009) 3146-3155.

[54] N. Sykam, G.M. Rao, Lightweight flexible graphite sheet for high-performance electromagnetic interference shielding, Materials Letters 233 (2018) 59-62.

[55] M.H. Al-Saleh, U. Sundararaj, X-band EMI shielding mechanisms and shielding effectiveness of high structure carbon black/polypropylene composites, Journal of Physics D: Applied Physics 46(3) (2013) 035304.

[56] M. Rahaman, T.K. Chaki, D. Khastgir, Development of high performance EMI shielding material from EVA, NBR, and their blends: effect of carbon black structure, Journal of Materials Science 46(11) (2011) 3989-3999.

[57] M.H. Al-Saleh, W.H. Saadeh, U. Sundararaj, EMI shielding effectiveness of carbon based nanostructured polymeric materials: A comparative study, Carbon 60 (2013) 146-156.

[58] S.-S. Hwang, Tensile, electrical conductivity and EMI shielding properties of solid and foamed PBT/carbon fiber composites, Composites Part B: Engineering 98 (2016) 1-8.

[59] D. Xing, L. Lu, W. Tang, Y. Xie, Y. Tang, An ultra-thin multilayer carbon fiber reinforced composite for absorption-dominated EMI shielding application, Materials

Letters 207 (2017) 165-168.

[60] S.C. Ryu, J.Y. Kim, C. Cho, W.N. Kim, Improvements of the Electrical Conductivity and EMI Shielding Efficiency for the Polycarbonate/ABS/Carbon Fiber Composites Prepared by Pultrusion Process, Macromolecular Research 28(2) (2019) 118-125.

[61] X. Luo, D.D.L. Chung, Electromagnetic interference shielding using continuous carbon-fiber carbon-matrix and polymer-matrix composites, Composites: Part B 30 (1999) 227-231.

[62] S. Geetha, K.K. Satheesh Kumar, C.R.K. Rao, M. Vijayan, D.C. Trivedi, EMI shielding: Methods and materials-A review, Journal of Applied Polymer Science 112(4) (2009) 2073-2086.

[63] X. Zhao, J. Fu, H. Wang, The electromagnetic interference shielding performance of continuous carbon fiber composites with different arrangements, Journal of Industrial Textiles 46(1) (2015) 45-58.

[64] W.S. Jou, A novel structure of woven continuous-carbon fiber composites with high electromagnetic shielding, Journal of Electronic Materials 33 (2004) 162-170.

[65] H. Mei, D. Han, S. Xiao, T. Ji, J. Tang, L. Cheng, Improvement of the electromagnetic shielding properties of C/SiC composites by electrophoretic deposition of carbon nanotube on carbon fibers, Carbon 109 (2016) 149-153.

[66] J. Wu, D.D.L. Chung, Increasing the electromagnetic interference shielding effectiveness of carbon fiber polymer-matrix, Carbon 40 (2002) 445-467.

[67] N.C. Das, T.K. Chaki, D. Khastgir, A. Chakraborty, Electromagnetic interference shielding effectiveness of conductive carbon black and carbon fiber-filled composites based on rubber and rubber blends, Advance in polymer technology 20 (2001).

[68] S.H. Lee, J.Y. Kim, C.M. Koo, W.N. Kim, Effects of processing methods on the electrical conductivity, electromagnetic parameters, and EMI shielding effectiveness of polypropylene/nickel-coated carbon fiber composites, Macromolecular Research 25(9) (2017) 936-943.

[69] C.-Y. Huang, W.-W. Mo, M.-L. Roan, The influence of heat treatment on

electroless-nickel coated fiber (ENCF) on the mechanical properties and EMI shielding of ENCF reinforced ABS polymeric composites, Surface and Coatings Technology 184(2-3) (2004) 123-132.

[70] S. Geetha, K.K.S. Kumar, C.R.K. Rao, M. Vijayan, D.C.J. Trivedi, EMI Shielding: Methods and Materials-A Review, Journal of Applied Polymer Science 112(4) (2010) 2073-2086.

[71] A.A. Eddib, D.D.L. Chung, The importance of the electrical contact between specimen and testing fixture in evaluating the electromagnetic interference shielding effectiveness of carbon materials, Carbon 117(Complete) (2017) 427-436.

[72] H.C. Chen, K.C. Lee, J.H. Lin, M. Koch, Comparison of electromagnetic shielding effectiveness properties of diverse conductive textiles via various measurement techniques, Journal of Materials Processing Technology 192(4) (2007) 549-554.

[73] S.T. Maciej Jaroszewski, Advanced Materials for Electromagnetic Shielding: Fundamentals, Properties, and Applications, 2018.

[74] F.H. Wee, P.J. Soh, A.H.M. Suhaizal, H. Nornikman, A.A.M. Ezanuddin, Free Space Measurement Technique on Dielectric Properties of Agricultural Residues at Microwave Frequencies, Microwave & Optoelectronics Conference, 2009.

[75] J.C. Moulder, E. Uzal, J.H. Rose, Thickness and conductivity of metallic layers from eddy current measurements, Review of Scientific Instruments 63(6) (1992) 3455-3465.

[76] Z. Li, Z. Meng, A Review of the Radio Frequency Non-destructive Testing for Carbon-fibre Composites, Measurement Science Review 16(2) (2016) 68-76.

[77] D. Wu, F. Cheng, F. Yang, C. Huang, Non-destructive testing for carbon-fiber-reinforced plastic (CFRP) using a novel eddy current probe, Composites Part B: Engineering 177 (2019) 107460.

[78] K. Mizukami, A.S.b. Ibrahim, K. Ogi, N. Matvieieva, I. Kharabet, M. Schulze, H. Heuer, Enhancement of sensitivity to delamination in eddy current testing of carbon fiber composites by varying probe geometry, Composite Structures 226 (2019) 111227.

[79] Y. He, G. Tian, M. Pan, D. Chen, Non-destructive testing of low-energy impact in

CFRP laminates and interior defects in honeycomb sandwich using scanning pulsed eddy current, Composites Part B: Engineering 59 (2014) 196-203.

[80] K. Mizukami, Y. Mizutani, A. Todoroki, Y. Suzuki, Analytical solutions to eddy current in carbon fiber-reinforced composites induced by line current, Advanced Composite Materials 25(4) (2015) 385-401.

[81] S. Jiao, J. Li, F. Du, L. Sun, Z. Zeng, Characteristics of Eddy Current Distribution in Carbon Fiber Reinforced Polymer, Journal of Sensors 2016 (2016) 1-8.

[82] A.M. Amaro, P.N.B. Reis, M.F.S.F. de Moura, J.B. Santos, Damage detection on laminated composite materials using several NDT techniques, Insight - Non-Destructive Testing and Condition Monitoring 54(1) (2012) 14-20.

[83] Q. Shen, M. Omar, S. Dongri, Ultrasonic NDE Techniques for Impact Damage Inspection on CFRP Laminates, Journal of Materials Science Research 1(1) (2011).

[84] A.M. Amaro, J.B. Santos, J.S. Cirne, Delamination Depth in Composites Laminates With Interface Elements and Ultrasound Analysis, Strain 47(2) (2011) 138-145.

[85] M. Kersemans, A. Martens, K. Van Den Abeele, J. Degrieck, F. Zastavnik, L. Pyl, H. Sol, W. Van Paepegem, Detection and Localization of Delaminations in Thin Carbon Fiber Reinforced Composites with the Ultrasonic Polar Scan, Journal of Nondestructive Evaluation 33(4) (2014) 522-534.

[86] M. Kusano, H. Hatano, M. Watanabe, S. Takekawa, H. Yamawaki, K. Oguchi, M. Enoki, Mid-infrared pulsed laser ultrasonic testing for carbon fiber reinforced plastics, Ultrasonics 84 (2018) 310-318.

[87] Jan-Carl Grager, Daniel Kotschate, Jakob Gamper, Mate Gaal, Katja Pinkert, Hubert Mooshofer, Matthias Goldammer, C.U. Grosse, Advances in air-coupled ultrasonic testing combining an optical microphone with novel transmitter concepts, 12th European conference on Non-Destructive Testing, Gothenburg, Sweden, 2018.

[88] Deepak K. Ghodgaonkar, Vasundara V. Varadan, V.K. Varadan, A free-space method for measurement of dielectric constants and loss tangents at microwave frequencies, IEEE Transactions on Instrumentation and Measurement 38(3) (1989)

789-793.

[89] V.V. Varadan, R.D. Hollinger, D.K. Ghodgaonkar, V.K. Varadan, Free-space, broadband measurements of high-temperature, complex dielectric properties at microwave frequencies, IEEE Transactions on Instrumentation and Measurement 40(5) (1991) 842-846.

[90] U.C. Hasar, Non-destructive testing of hardened cement specimens at microwave frequencies using a simple free-space method, NDT & E International 42(6) (2009) 550-557.

[91] M. Ozturk, U.K. Sevim, O. Akgol, M. Karaaslan, E. Unal, An electromagnetic non-destructive approach to determine dispersion and orientation of fiber reinforced concretes, Measurement 138 (2019) 356-367.

Chapter 2

Electromagnetic interference shielding anisotropy enhanced by CFRP laminated structures

2 Electromagnetic interference shielding anisotropy enhanced by CFRP laminated structures

2.1 Introduction

Rapid developments in technology have increased people's exposure to EM radiation emitted from various electronic products. Some sensitive equipment may also be subject to electromagnetic compatibility (EMC) problems when exposed to EM radiation [1-3]. EM waves can come from natural sources, such as lighting, and EM waves emitted by relays and fluorescent lights can interfere with the performance of electronics and electrical devices by generating noise [4, 5]. In addition to EMC problems, exposure to EM radiation at a specific bandwidth for long periods may negatively impact human health by causing cancer, heart problems, asthma, and miscarriages [6]. Various EMI shielding materials have been developed in recent decades, and interest in developing novel and more efficient materials is growing.

Conductive metallic materials, including brass and stainless steel, were initially considered suitable for EMI shielding. However, they are not appropriate for some industrial applications. This is because their corrosion resistance is poor, and the materials are dense and inflexible [7]. Composites reinforced with metallic fillers such as fibers and nanoparticles, have thus been developed to replace them [8-11]. Carbon-based materials are excellent electrical fillers. Examples of carbon-based materials

include graphite [12, 13], carbon nanotubes [14, 15], carbon nanofibers [16], and graphene [17] . Their optimal electrical properties make them good EMI shielding materials. Carbon-based polymer composites overcome many of the drawbacks of metallic materials, and they have unique EMI shielding properties [18-22]. Wen et al. [23] fabricated anisotropic PVB/Ni-graphite/short-cut carbon fiber film to achieve high EMI shielding performance, and the results showed that the films had excellent anisotropic SE. Production of these materials requires little energy, and they are flexible, machinable, and low in weight.

Composites reinforced with conventional short and continuous carbon fibers are important materials for many aerospace and automotive applications, and they are also used to manufacture sports equipment. They are strong, thermally conductive, and highly processable materials with moduli [24]. Continuous carbon fiber reinforced composites possess excellent electrical conductivity in the fiber direction, which is critical for achieving good EMI shielding performance. Short carbon fibers can be used as fillers to generate three-dimensional conductive networks, which are advantageous for EM wave attenuation. The addition of nanofiller (nanoparticles, nanotubes, graphene) to composites further enhances the electrical conductivity network, consequently improving the attenuation of EM waves. In summary, research on carbon-reinforced composites for EMI shielding has focused primarily on material modifications, and there are few reports on structural adjustment.

Continuous carbon fibers have excellent electrical properties. The electrical properties of anisotropic and quasi-isotropic composites, including electrical

conductivity and permittivity, are directionally dependent. This is a key feature of composites that effectively shield against EM radiation. EM waves are composed of both electric and magnetic fields, which tend to be polarized during wave propagation. The electrical properties of the surfaces of homogeneous materials, such as metals, are the same in each direction. Thus, the location on the material selected for measurement has no effect on the results. The EMI shielding performance of continuous carbon fiber composites with anisotropic electrical properties is strongly influenced by the angle between the fibers and the direction of EM wave polarization. Some reports [25-27] indicated that the EMI shielding performance of CFRP could be affected by the fiber orientation, array spacing and overlap angle. However, few studies focused on the investigation of the relationship between EMI shielding performance and the angle of electric field and fiber direction. Meanwhile, the mechanism of the improved shielding performance by structural adjustment was also not elaborated theoretically.

Generally, four methods are used to evaluate EMI shielding properties, namely the transmission line, shielded box, shield room, and free space methods [28]. The transmission line method is currently the most widely used electromagnetic shielding test method. According to ASTM Standard Method D4935, testing must be performed using annular samples with specific outer and inner diameters. This method allows the reflection, absorption, and transmission components of overall shielding to be determined separately. Eddib et al. [29] have shown that the electrical contact between a sample and the testing apparatus directly affects the results of EMI shielding tests. The coaxial transmission line method is currently recognized as a standard method for

measuring planar shielding [30]. Since the electric field of EM waves are distributed radially on the surface of the material inside the coaxial tube, coaxial transmission line measurement are always performed to evaluate the EMI shielding performance of homogeneous materials. It is necessary to pay close attention to the influence of EM wave polarization on experimental results, but there are few reports on it.

In order to clarify the EMI shielding anisotropy of CFRP composites, we tried to use the coaxial transmission line method to measure the EMI SE of CFRP laminated structures with different fiber orientations. CFRP composites with various layup configurations were fabricated as cost-effective EMI shielding materials. In this chapter, the effects of carbon fiber type, the number of layers, and fiber orientation on the EMI shielding properties of the CFRP composites were investigated.

2.2 Experimental

2.2.1 Materials

Pitch-based XN80, XN60, and XN05 continuous carbon fiber prepregs and a T700S PAN-based continuous carbon fiber prepreg were supplied by Nippon Graphite Fiber Co., Ltd. (Hyogo Prefecture, Japan) and Nippon Oil & Energy Corp (Tokyo, Japan). Each prepreg had an areal density of 125g·m^{-2}, and the fiber diameter is about 10μm. The fundamental carbon fiber parameters are shown in Table 2.1.

Table 2.1 Properties of the carbon fibers

Fibers	Tensile strength (MPa)	Tensile Modulus (GPa)	Density ($g \cdot cm^{-3}$)	Electric Resistivity ($10^{-4}\Omega \cdot cm$)
XN80	3,430	780	2.12	5
XN60	3,430	620	2.12	7
XN05	1,130	53	1.65	2.8
T700S	4,900	230	1.8	16

2.2.2 Composite fabrication

To determine the effect of fiber layup configurations on the EMI shielding of CFRP composites, we fabricated XN80-based CFRP samples with four different cross-layered fiber configurations, which were designated (0°/0°/0°/0°), (0°/0°/90°/90°), (0°/90°/0°/0°), and (0°/90°/0°/90°) (Fig. 2.1 (a)). Each specimen was cured for 1.5 h at 135 °C and 2 MPa using a hot press. All of the samples with four layers were approximately 0.55 mm thick, where the thickness of each layer is 0.138 mm. They were shaped into concentric tubes with outer and inner diameters of 13 mm and 1.7 mm, respectively (Fig. 2.1 (b)), to perform coaxial transmission line measurements.

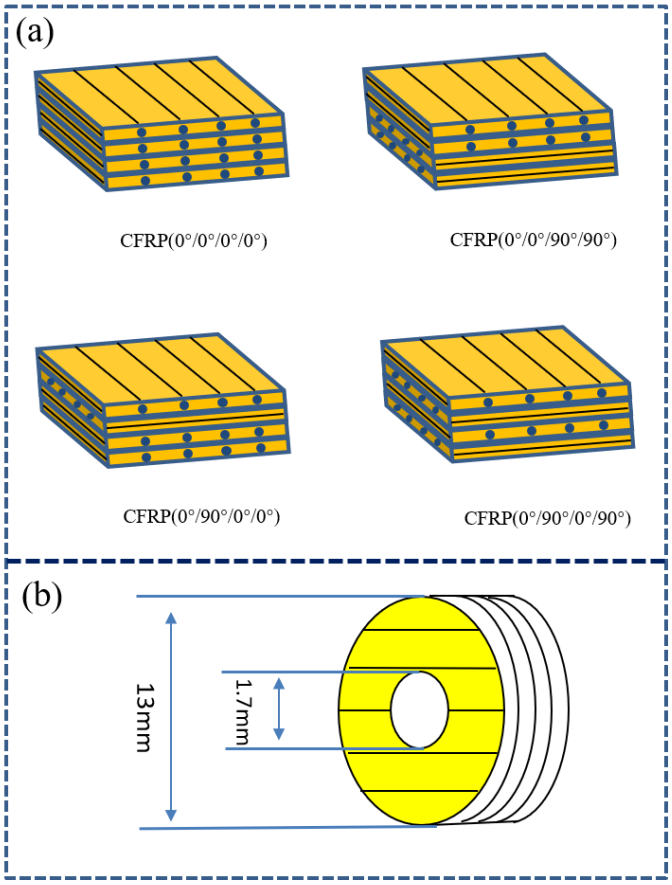

Fig. 2.1 (a) Schematic diagrams showing the alignment of fibers in each of the four CFRP, and (b) Schematic diagram of sample for coaxial transmission line testing.

2.2.3 Electrical conductivity measurement

The electrical conductivity of each reinforced carbon fiber composite was measured using a four-probe configuration. Current was applied to the two outer probes, and the resulting voltage drop was measured using the two inner probes. In contrast to the two-point configuration, measurements performed using the four-probe configuration are not affected by contact resistance. Silver paste was used to form good contacts between the electrodes and the CFRP composites to ensure accuracy. The electrical conductivity (σ) was calculated using Eq. (1).

$$\sigma(s/m) = \frac{L}{RS} = \frac{IL}{US} \quad (1)$$

where I is the applied current, U is the obtained voltage, S is the cross-sectional area, and L is the distance between the two voltage probes.

2.2.4 EMI shielding mechanisms

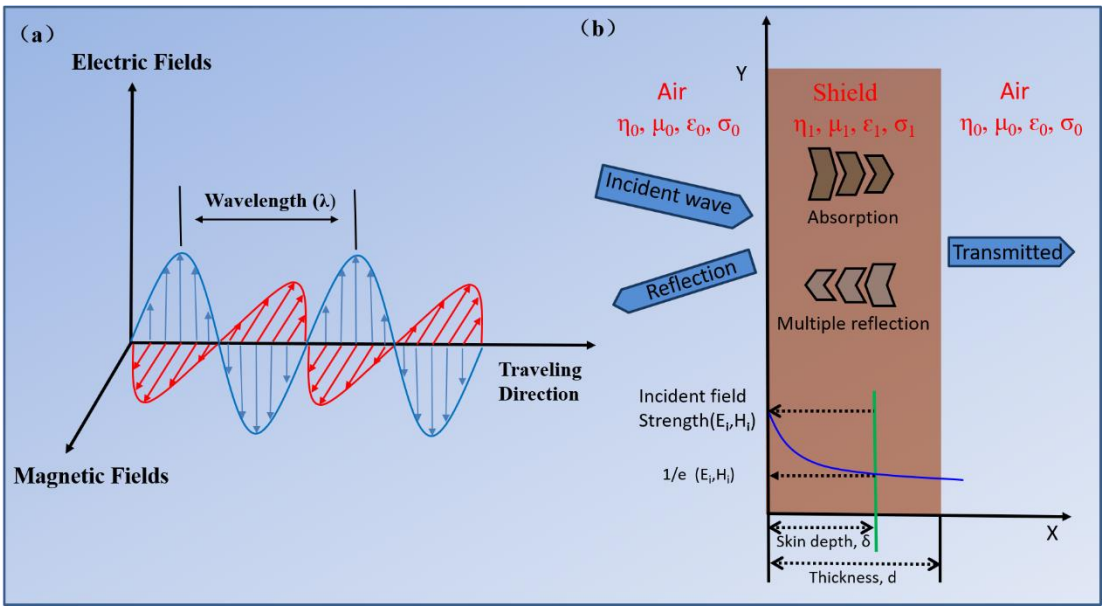

Fig. 2.2 Schematic representation of (a) EM waves propagation, and (b) EMI shielding mechanisms.

Electromagnetic waves propagate at the speed of light (υ) in a vacuum. The oscillating electric and magnetic fields are perpendicular to each other and to the direction of the EM wave, referred to as a transverse wave (Fig. 2.2 (a)). The primary EMI shielding mechanisms (Fig. 2.2 (b)) are reflection (SE_R), absorption (SE_A), and multiple reflection (SE_M). When an EM wave encounters the surface of a material, a portion is reflected due to the mismatch between the impedances of the medium and the shield. Reflection is dominated by the mobile charge carriers in the material [31]. Electrical conductivity has been proved a critical factor associated with the EMI shielding effect [16]. The electrical conductivity of a material depends on a continuous

conduction pathway. Although a continuous conduction pathway is not required for EM shielding, it can enhance the shielding performance of a material [32]. EM waves entering the interior of a composite can interact with magnetic and/or electric dipoles and be converted into other forms of energy, such as heat [33]. This shielding process is known as absorption. Electrical and magnetic dipoles form only in materials with high permittivity and permeability [34]. Multiple reflections are attributed to the surfaces and interfaces in porous and foam composites and to reinforcing fillers with large surface areas [32]. However, multiple reflections can be ignored when the absorption (SE_A) exceeds 15 dB [35].

Shielding effectiveness can be calculated using Eq. (2). Derivation of the SE equation according to EMI shielding theory is shown below.

$$\begin{aligned} SE &= -20\log_{10}|T| \\ &= 20\log_{10}\left|e^{rd}\right| - 20\log_{10}|p| + 20\log_{10}\left|1 - qe^{-2rd}\right| \\ &= 8.68\frac{d}{\delta} + 20\log_{10}\frac{|K+1|^2}{4|K|} + 20\log_{10}\left|1 - \frac{(K-1)^2}{(K+1)^2}e^{-2rd}\right| \\ &= SE_A + SE_R + SE_{MR} \end{aligned} \tag{2}$$

The variables *r*, *d*, *p*, and *q* represent the propagation constant, shield thickness, the transmission coefficient, and the reflection coefficient, respectively. *k* is the ratio of the EM wave and shield material impedance values, and δ is the skin depth of the shield.

The skin depth is defined as the distance between the shield surface and the point at which the electric field strength is equal to 1/e of its incident value (Fig. 2.2 (b)). The skin depth can be calculated using Eq. (3).

$$\delta = 1/\sqrt{\pi\mu f\sigma} \tag{3}$$

Where μ represents magnetic permeability, f is the frequency, and σ is the electrical conductivity.

The absorption component of shielding efficiency (SE_A) can be expressed by rewriting the shielding efficiency equation as shown in Eq. (4).

$$SE_A = 8.68d\sqrt{\pi\mu f\sigma} \tag{4}$$

According to Eq. (4), the absorption capacity of the shielding material increases with increasing frequency and electrical conductivity. The absorption loss can be improved by increasing the thickness of the shield.

According to the definition, the reflection formula can be expressed as shown in Eq. (5).

$$SE_R = 20\log_{10}\frac{|K+1|^2}{4|K|} = 20\log_{10}\frac{\left|\frac{\eta_0}{\eta_1}+1\right|^2}{4\left|\frac{\eta_0}{\eta_1}\right|} \tag{5}$$

where η_1 and η_0 are the intrinsic impedances of the two different mediums through which the EM waves pass. The values of SE_R when $\eta_1 \gg \eta_0$ and $\eta_1 \ll \eta_0$, are obtained using Eq. (6).

$$SE_R = 20\log_{10}\frac{1}{4}\left|\frac{\eta_1}{\eta_0}\right| \text{ , } \eta_1 \gg \eta_0 \tag{6}$$

$$SE_R = 20\log_{10}\frac{1}{4}\left|\frac{\eta_0}{\eta_1}\right| \text{ , } \eta_1 \ll \eta_0$$

Eq. (6) shows that reflection can occur when an electromagnetic wave encounters the interface between two mediums with different intrinsic impedances. The greater the difference between η_1 and η_0, the more effectively electromagnetic waves will be reflected at the interface.

2.2.5 Measurement of EMI shielding effectiveness

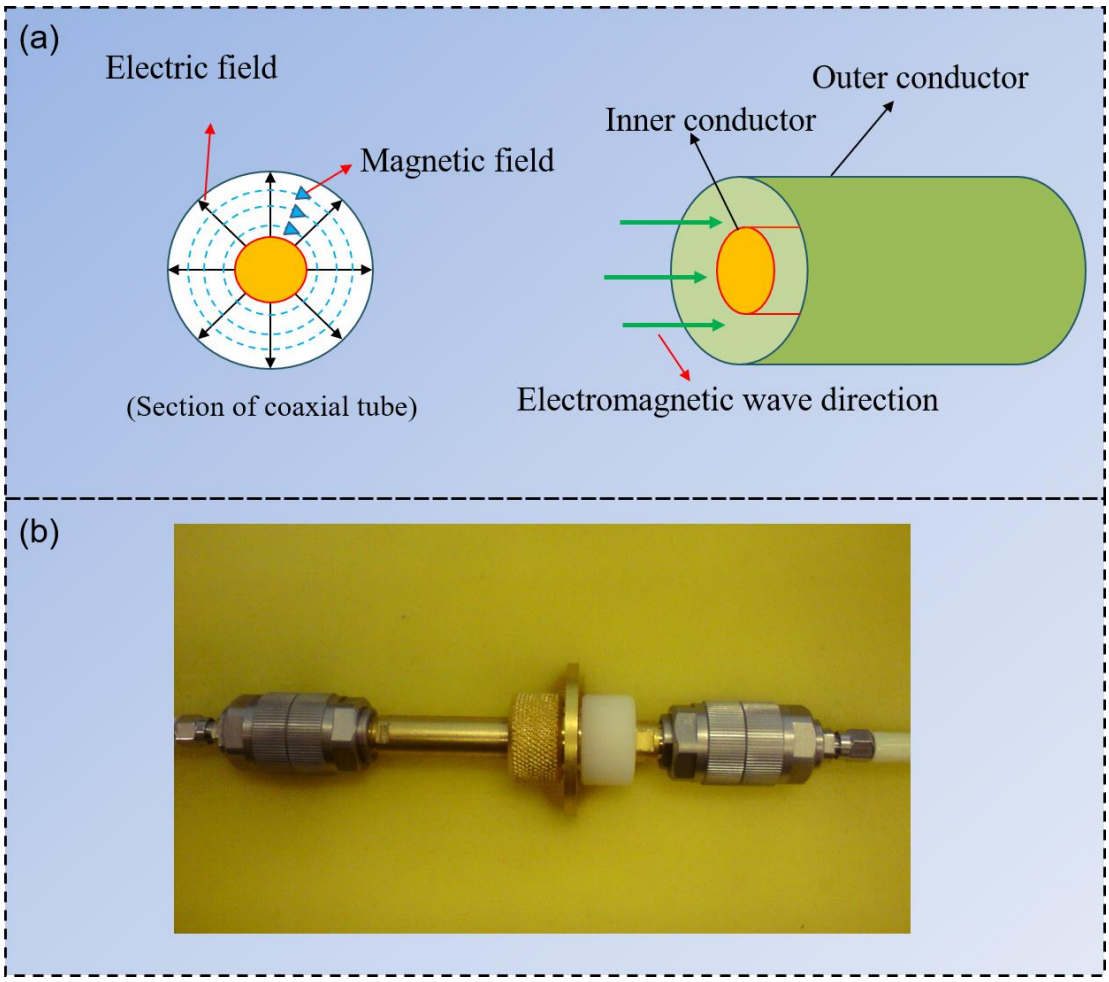

Fig. 2.3 Schematic illustration showing the electric field distribution within a (a) coaxial tube, and (b) the coaxial setup used for the SE measurements.

We measured the EMI shielding efficiencies of the CFRP composites using the coaxial transmission line method. The testing apparatus (Fig. 2.3) consisted of a coaxial waveguide and a vector network analyzer connected by GPIB cables. This method theoretically allows operation at frequencies up to 1.5 GHz based on the testing system dimensions in the ASTM D4935-99 Standard Method [29]. The apparatus used in this work contained an outer conductor and an inner conductor. Theoretically, we could measure SE at frequencies up to 18 GHz. Prior to measuring the shielding effectiveness of the specimens, the testing system was calibrated using a calibration kit.

The scattering (S) parameters were determined using the coaxial testing system. The $S_{12}(S_{21})$ and $S_{11}(S_{22})$ parameters are related to the transmission coefficient and the reflection coefficient, respectively. Eq. (7) shows the relationships between transmittance (T), reflectance (R), absorptivity (A), and the $S_{12}(S_{21})$ and $S_{11}(S_{22})$ parameters.

$$T = |S_{21}|^2 = |S_{12}|^2 \tag{7}$$

$$R = |S_{11}|^2 = |S_{22}|^2$$

$$A = 1 - R - T$$

The shielding effectiveness of reflection (SE_R) and the total shielding (SE_T) are calculated by the following formulae:

$$SE_R = -10\log(1 - |S_{11}|^2) = -10\log(1 - |S_{22}|^2) \tag{8}$$

$$SE_T = -10\log(|S_{21}|^2) = -10\log(|S_{12}|^2) \tag{9}$$

The absorption SE (SE_A) can be described as:

$$SE_A = SE_T - SE_R \tag{10}$$

EMI SE can also be calculated using Eq. (11) based on the incident and transmitted EM power, which includes the power of the magnetic and electric fields.

$$\text{EMI SE} = 10\log\left(\frac{P_T}{P_I}\right) = 20\log\left(\frac{E_T}{E_I}\right) = 20\log\left(\frac{H_T}{H_I}\right) \tag{11}$$

where P_I and P_T represent the intensities of the incident and transmitted radiation. E_T and E_I represent the intensities of the electric field for the incident and transmitted radiation, H_T and H_I are the intensities of the incident and transmitted magnetic fields.

2.3 Results and discussion

2.3.1 EMI shielding anisotropy of CFRP

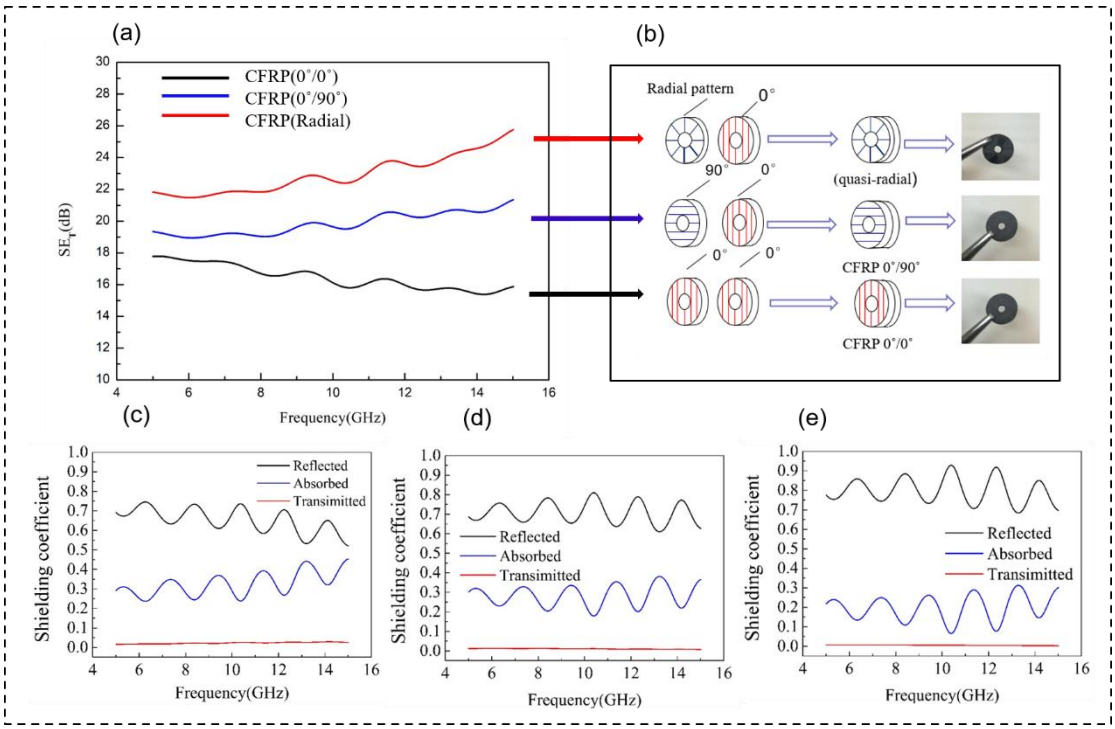

Fig. 2.4 (a) Shielding effectiveness of CFRP composites with different fiber orientations; (b) schematic illustrations of the fiber distributions in the CFRP composites; (c) shielding coefficients of the CFRP (0°/0°); (d) CFRP (0°/90°); and (e) quasi-radial CFRP samples.

Table 2.2 EMI SE of CFRP composites with different fiber orientation at 15 GHz.

Sample	Reflection SE (SE_R, dB)	Absorption SE (SE_R, dB)	Total SE (dB)
CFRP (0°/0°)	3.2	12.7	15.9
CFRP (0°/90°)	4.3	17.1	21.4
CFRP (radial)	5.2	20.6	25.8

Our first aim was to investigate CFRP EMI shielding anisotropy using the coaxial transmission line method. We fabricated three CFRPs with fibers in three different orientations. The CFRP (0°/0°), CFRP (0°/90°), and quasi-radial CFRP arrangements

are illustrated in Fig. 2.4(b). All three samples were two-ply with unidirectional carbon prepreg base layers and thicknesses of 0.27 mm. The prepregs used to fabricate the quasi-radial sample were cut into several pieces and combined to form a quasi-radial structure. The overall EMI shielding efficiencies of the three CFRP composites are plotted against the frequency in Fig. 2.4(a). The SE of the CFRP (0°/90°) and CFRP (radial) samples increased as the frequency increased. However, the SE of the CFRP (0°/0°) sample decreased.

The shielding coefficients of the CFRP (0°/0°), CFRP (0°/90°), and CFRP (radial) samples are plotted against the frequency in Fig. 2.4(c)-(e). Shielding by reflection decreased as the frequency increased, but the absorption showed the opposite trend for CFRP (0°/0°), as shown in Fig. 2.4(c). Since the decrease in its reflection coefficient was greater in magnitude than the increase in its absorption coefficient, the overall SE of the CFRP (0°/0°) composite decreased. These results indicated that reflection was the primary mechanism of EMI shielding. The contribution of reflection to EMI shielding increased as the composite structure changed, and the quasi-radial CFRP composite reflected the most EM radiation. We attributed this primarily to the quasi-radial distribution of the carbon fibers, which aligned strongly in the direction of the electrical field (Fig. 2.3).

The CFRP (radial) composite exhibited the best EMI shielding performance, and its SE was approximately 25.8 dB at 15 GHz (Table 2.2). The EMI shielding performance of the CFRP (0°/0°) sample was the poorest of the three, and its SE was only 15.9 dB at the same frequency. Changing the carbon fiber orientation resulted in

enhanced reflection and absorption by the CFRP (0°/90°) and quasi-radial CFRP samples. The shielding by reflection (SE_R) values of the CFRP (0°/0°), CFRP (0°/90°), and CFRP (radial) samples were 3.2 dB, 4.2 dB, and 5.2 dB, respectively (Table 2.2). According to Eq. (7), this meant that the CFRP (0°/0°), CFRP (0°/90°), and CFRP (radial) samples reflected 52%, 62.7%, and 69.6% of the total EM radiation, respectively. The SE_A values of the CFRP (0°/0°), CFRP (0°/90°), and CFRP (radial) samples (Table 2.2) indicated that they absorbed 94.7%, 98.1%, and 99.1%, respectively, of the non-reflected EM radiation. However, the samples absorbed only 45.4%, 36.5%, and 30.1% of the overall incident EM radiation. We thus concluded that reflection was the dominant EMI shielding mechanism, and that overall SE could be improved by optimizing the composite structure.

When an electromagnetic wave propagates from one medium to another, it will be reflected at the interface if the difference between η_1 and η_0 is large. The intrinsic impedance of a medium can be expressed using Eq. (12).

$$\eta = \sqrt{\frac{j\omega\mu}{\sigma+j\omega\varepsilon}} = \sqrt{\frac{2\pi j\mu f}{\sigma+j\omega\varepsilon}} \quad (12)$$

where μ, f, σ, and ε represent the magnetic permeability, frequency, electrical conductivity, and electric permittivity, respectively. These parameters govern the impedance value of the material. For poor conductivity materials, such as air ($\sigma = 0$), the Eq. (13) can be used to calculate η.

$$\eta = \sqrt{\frac{\mu}{\varepsilon}} \quad (13)$$

For materials with good conductivity, where $\sigma \gg \omega\varepsilon$, the formula can be expressed as:

$$\eta = (1 + \mathrm{j})\sqrt{\frac{\pi\mu f}{\sigma}} \tag{14}$$

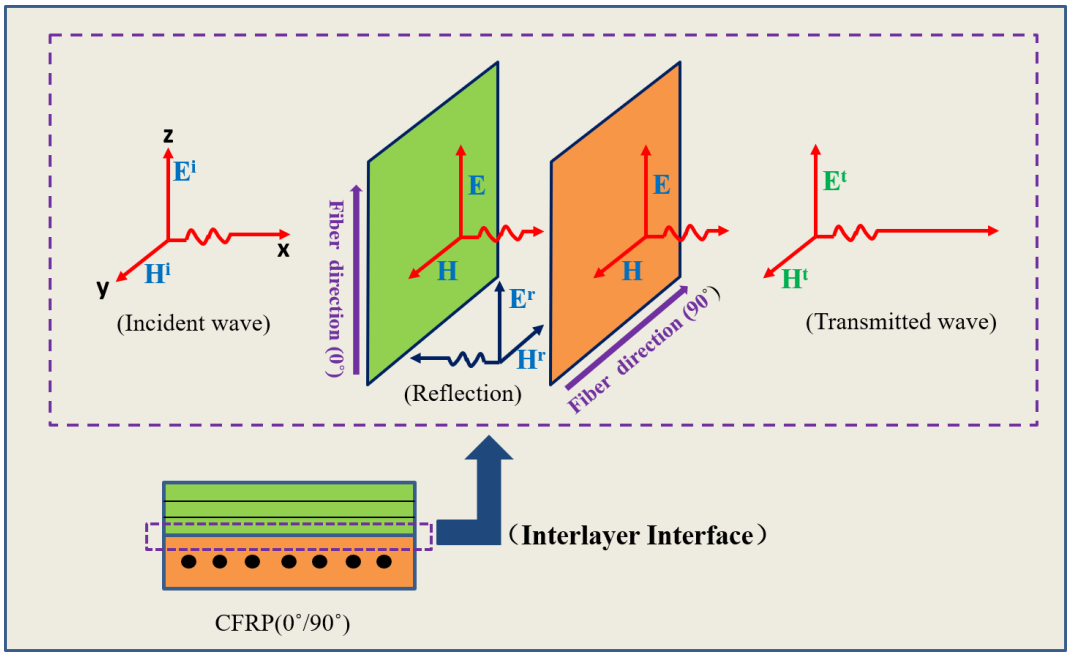

Fig. 2.5 Schematic diagram of EM reflection at the interlayer interface of CFRP(0°/90°)

The anisotropic properties of the CFRP (0°/0°) composite were due to the unidirectional orientation of the carbon fibers within the sample. Its anisotropic properties included electrical conductivity, electrical permittivity, and mechanical anisotropy. Many researchers have shown that the conductivity and electrical permittivity of unidirectional CFRP composites vary depending on the direction in which they are measured. EM waves encounter an interface between two layers with differing fiber orientations, such as those in the CFRP (0°/90°) composite. The fibers in the first CFRP layer (0°) aligned with the electric field, but the field was perpendicular to the fibers in the second layer (Fig. 2.5). CFRPs with different fiber arrangements will exhibit different electrical properties in the same electric field direction. The electrical resistance values along the fibers is far lower than that perpendicular to the fibers in the unidirectional CFRP composite. The impedance values

also differed according to Eq. (12).

EM waves were reflected at the interfaces within the CFRP (0°/90°) and CFRP (radial) composites according to Eq. (6), which was consistent with the experimental results. These composites reflected EM radiation more effectively than the CFRP (0°/0°) sample, and their overall shielding efficiencies were higher. The differences between the impedance values of the layers in the CFRP (0°/90°) and CFRP (radial) composites were larger due to their cross-layered fiber configurations. Reflection and absorption occurred within the materials, which enhanced their overall EMI shielding performance. This was why the EMI SE of the CFRP (0°/90°) composite was superior to that of the unidirectional material. The electric field was distributed radially on the surfaces of the samples within the coaxial tubes. Relative to the fibers in the CFRP (0°/90°) composite, the carbon fibers in the CFRP (radial) composite aligned more completely with the electric field. Only a portion of the fibers in the CFRP (0°/90°) composite aligned with the electric field. This was why the CFRP (radial) composite reflected and absorbed more effectively than the CFRP (0°/90°) composite, even though their thicknesses were nearly identical. The internal fibers were cross-laminated, so internal reflection and absorption by the cross-ply CFRP composites were more efficient than they were in the unidirectional CFRP material. The EMI shielding performance of the three samples followed the order CFRP (radial) > CFRP (0°/90°) > CFRP (0°/0°).

We also found that the EMI SE of each material did not vary if the composite was rotated along the axis of the inner conductor in the coaxial apparatus. However, the angle between the electric field and the fiber direction affected the EMI shielding

measurements. EMI shielding variations must thus be considered when the coaxial tube method is used to evaluate the shielding performance of a continuous carbon fiber reinforced composite.

2.3.2 Effects of carbon fiber types on EMI shielding performance

To study the influence of carbon fiber composition on EMI SE, we prepared anisotropic composites using XN80, XN05, XN60, and T700S carbon fibers. All the samples have the same thickness of 0.55mm. The EM shielding properties of the composites were evaluated using the coaxial transmission line method. The results are shown in Fig. 2.6. The T700S-based composite had the lowest SE, while the XN05-based CFRP composite provided the most EMI shielding. This was attributed to the difference between the electrical conductivities of the CFRP composites. The impedance value of a highly conductive CFRP composite differs significantly from that of air. When electromagnetic radiation in the atmosphere enters a highly conductive CFRP, the EM waves will be reflected at the interfaces. According to Eq. (3), an incremental increase in conductivity reduces the skin depth of CFRP.

The electrical conductivities of the CFRPs reinforced with different carbon fibers are compared in Fig. 2.7. The conductivity of the XN05-based CFRP was excellent, while the T700S-based CFRP was the poorest electrical conductor. These results were consistent with the results of the EMI SE measurements.

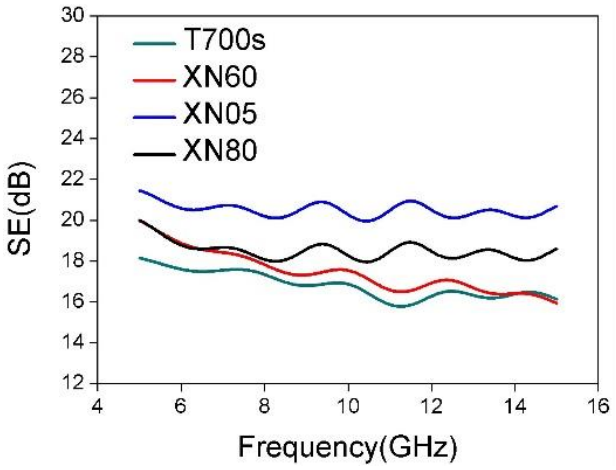

Fig. 2.6 SEs of CFRP composites containing different carbon fibers.

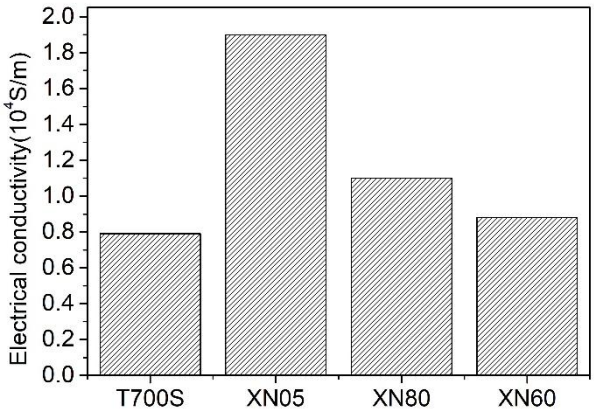

Fig. 2.7 Electrical conductivity of CFRPs with different fiber types in the fiber length direction.

2.3.3 Effects of fiber orientation patterns on EMI shielding performance of CFRP

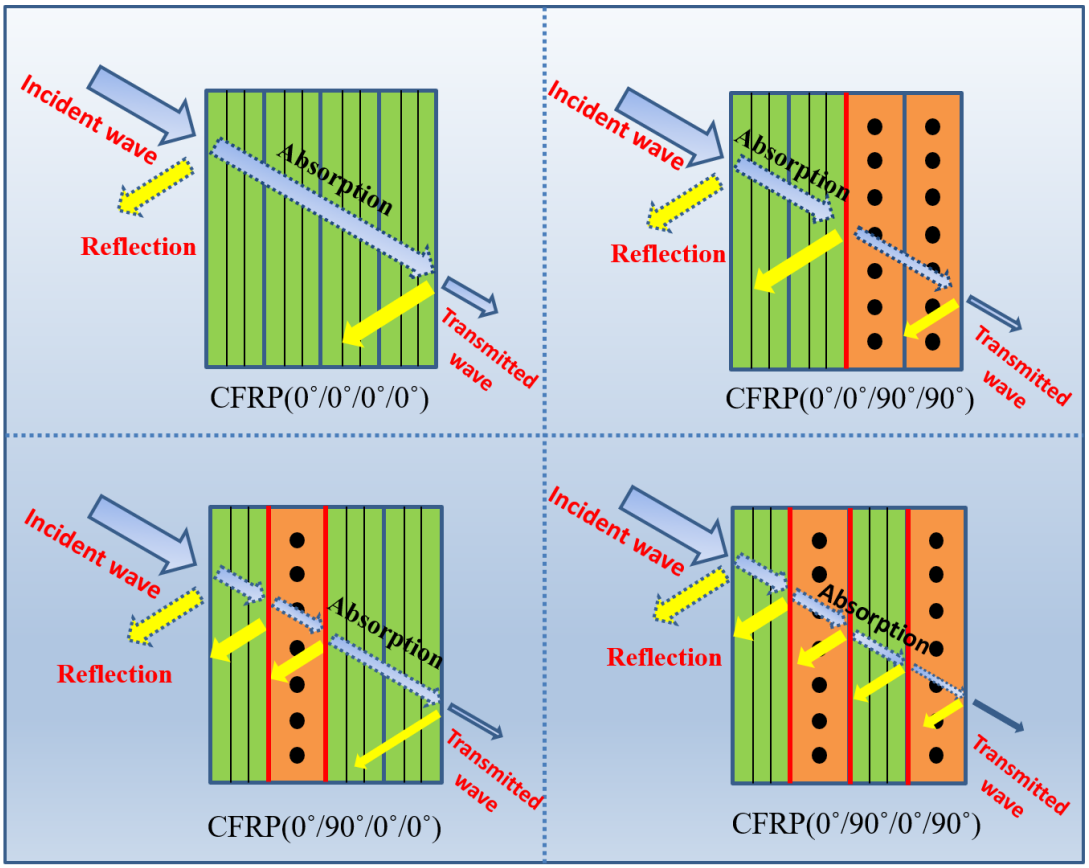

Fig. 2.8 Schematic illustrations of internal reflection in CFRP composites with different structures

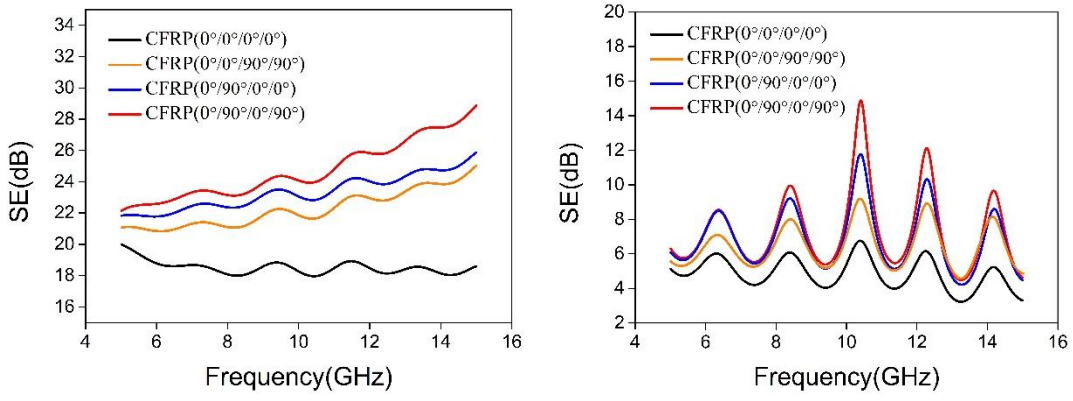

(a) (b)

Fig. 2.9 EMI shielding effectiveness of CFRP with different fiber orientation patterns: (a) total SE, and (b) reflective SE.

To investigate the influence of fiber orientation on the EMI shielding properties of

the carbon fiber prepreg composites, we fabricated CFRP composites with four different layer configurations. These were designated CFRP (0°/0°/0°/0°), CFRP (0°/0°/90°/90°), CFRP (0°/90°/0°/0°), and CFRP (0°/90°/0°/90°). The carbon fibers in the CFRP (0°/0°/0°/0°) sample were parallel to each other, while the other three CFRP composites had different layered configurations. The unidirectional and cross-layered configurations of the composites are illustrated schematically in Fig. 2.8. The total SEs of the CFRP samples are plotted in Fig. 2.9(a). The EMI SE of the CFRP (0°/0°/0°/0°) sample decreased slightly as the frequency increased, whereas the SE of the other three samples followed an opposite trend. The CFRP (0°/90°/0°/90°) sample had three cross-layers, and it had the highest SE (28.9 dB) at 15 GHz. This meant that the material shielded against up to 99.9% of the EM radiation. The SE of this material was far greater than that of the CFRP (0°/0°/0°/0°) sample (18.5 dB). The reflective SEs of the CFRP composites are shown in Fig. 2.9(b). The results confirmed that reflection was the primary mechanism of shielding, and that the ability of the materials to reflect electromagnetic waves was enhanced by cross-layering without changing the overall thickness.

The EM shielding performance of the cross-ply CFRP materials was superior to that of the unidirectional CFRP for two reasons. Fibers in the cross-ply materials were oriented in the 0° and 90° directions, while fibers in the unidirectional CFRP were aligned in a single direction. Since the electric field was distributed radially within the coaxial tubes, the EMI shielding performance of the cross-ply materials was better. This could be explained by the fact that electromagnetic shielding occurred primarily along

the direction of the fibers in each CFRP composite. We previously observed that a CFRP (0°/90°) cross-ply composite provided more shielding than a unidirectional CFRP material, which confirmed that cross-layering could enhance reflection and absorption. As shown in Fig. 2.8, four different layer configuration of CFRP (0°/0°/0°/0°), CFRP (0°/0°/90°/90°), CFRP (0°/90°/0°/0°), and CFRP (0°/90°/0°/90°) have 0, 1, 2 and 3 cross-layers inside the composites, respectively. When the EM waves encountered a cross layer, they were reflected due to the mismatch between the impedance values of the two layers. The EMI shielding performance of the cross-ply CFRP composites improved as the number of cross-layers increased, and the CFRP (0°/90°/0°/90°) composite with three cross-layers provided the best shielding.

The EMI SE of the CFRP (0°/90°/0°/90°) composite was 20% higher than that of the CFRP (0°/0°/90°/90°) composite at 15GHz. The samples contained an equal number of fibers in the 0° and 90° directions, and their thicknesses were essentially the same. The most significant difference between the CFRP composites was the number of cross-layers in the samples. The CFRP (0°/90°/0°/90°) composite contained three cross-layers, while the CFRP (0°/0°/90°/90°) contained only one. It can be confirmed that the number of cross-layers dominates the EMI shielding performance of CFRP.

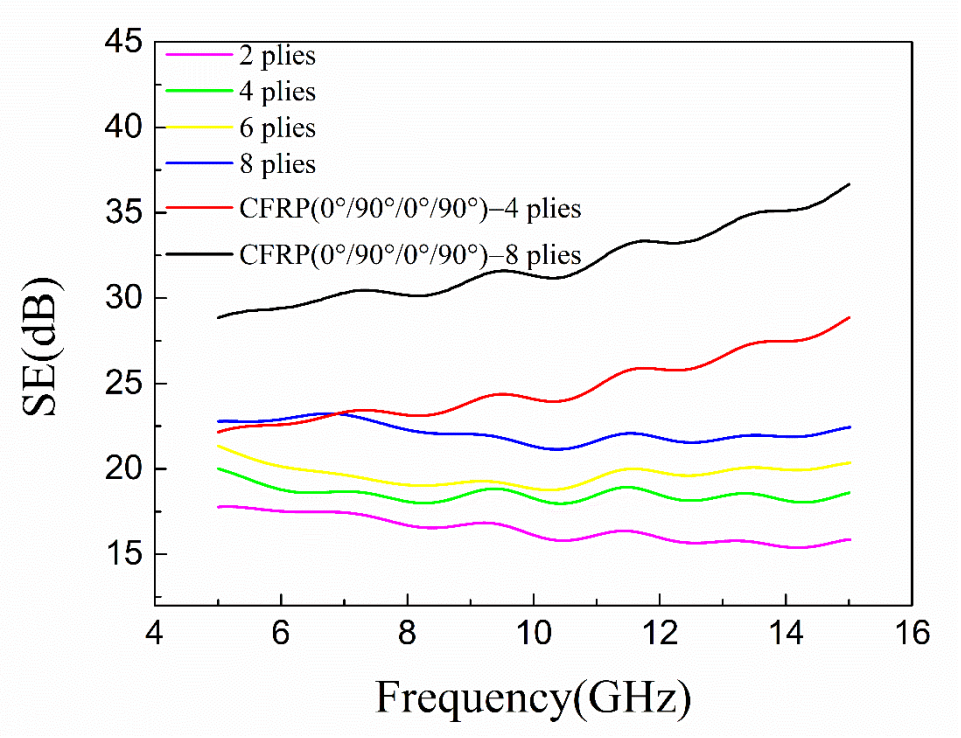

Fig. 2.10 EMI SE of CFRP with different layer numbers.

The EMI shielding performance related to different layer numbers is shown in Fig. 2.10. The eight-ply cross-layered CFRP composite shows high EMI shielding performance, far superior to that of the eight-ply unidirectional CFRP composite. Besides, the four-ply CFRP (0°/90°/0°/90°) composite obtained the SE (28.9 dB) at 15 GHz, which was even much higher than the SE of the eight-ply unidirectional CFRP composite (22.6 dB). It could thus be concluded that the number of cross layers in the composites governed their electromagnetic shielding performance. Hence, cost effective and efficient EMI shielding can be achieved by selecting a structure with an optimal fiber arrangement.

2.4 Conclusions

The optimization of EMI shielding performance of CFRP by changing the

composites' structure were investigated systematically. The effect of the angle between the direction of fibers in anisotropic CFRP and the electric field on the EMI shielding performance was clarified. The anisotropy of EMI shielding was confirmed for the first time by the coaxial transmission line method. The results showed that a quasi-radial sample had the highest shielding effectiveness (25.8 dB) at 15 GHz with the carbon fibers aligned in the direction of the electric field of EM waves. It is found that the orientation of fibers relative to the direction of electric field clearly affected the EMI shielding performance of the CFRP composites. The four-ply CFRP (0°/90°/0°/90°) with three cross-layers had the excellent shielding value of 28.9 dB at 15 GHz, that was far superior to that of a unidirectional CFRP (0°/0°/0°/0°) composite (SE= 18.6 dB), and this indicated the laminated structures governed SE, and the number of cross-layers in the composites also affected their EMI shielding performance. The shielding mechanisms of cross-layer CFRPs were also discussed and clarified based on both experimental and theoretical analysis. We believe that these findings could provide a scientific basis and potential in designing high-performance EMI shielding materials.

References

[1] S. Midya, R. Thottappillil, An overview of electromagnetic compatibility challenges in European Rail Traffic Management System, Transportation Research Part C Emerging Technologies 16(5) (2008) 515-534.

[2] G.Y. Slepyan, A. Boag, V. Mordachev, E. Sinkevich, S. Maksimenko, P. Kuzhir, G. Miano, M.E. Portnoi, A. Maffucci, Nanoscale Electromagnetic Compatibility: Quantum Coupling and Matching in Nanocircuits, IEEE Transactions on

Electromagnetic Compatibility 57(6) (2015) 1645-1654.

[3] M.K.E.B. Wallin, M. Therese, P.K. Hakansson, Modern wireless telecommunication technologies and their electromagnetic compatibility with life-supporting equipment, Anesthesia & Analgesia 101(5) (2005) 1393-1400.

[4] C.R. Paul, Introduction to Electromagnetic Compatibility John Wiley & Sons, Inc.,, Canada, 2006.

[5] D. Jiang, V. Murugadoss, Y. Wang, J. Lin, T. Ding, Z. Wang, Q. Shao, C. Wang, H. Liu, N. Lu, R. Wei, A. Subramania, Z. Guo, Electromagnetic interference shielding polymers and nanocomposites - A review, Polymer Reviews 59(2) (2019) 280-337.

[6] A. Joshi, A. Bajaj, R. Singh, A. Anand, P.S. Alegaonkar, S. Datar, Processing of graphene nanoribbon based hybrid composite for electromagnetic shielding, Composites Part B Engineering 69(69) (2015) 472-477.

[7] H. Abbasi, M. Antunes, J.I. Velasco, Recent advances in carbon-based polymer nanocomposites for electromagnetic interference shielding, Progress in Materials Science 103 (2019) 319-373.

[8] C.S. Chen, W.R. Chen, S.C. Chen, R.D. Chien, Optimum injection molding processing condition on EMI shielding effectiveness of stainless steel fiber filled polycarbonate composite International Communications in Heat & Mass Transfer 35(6) (2008) 744-749.

[9] R. Bagwell, J. McManaman, R. Wetherhold, Short shaped copper fibers in an epoxy matrix: Their role in a multifunctional composite, Composites Science and Technology 66(3-4) (2006) 522-530.

[10] M. Jalali, S. Dauterstedt, A. Michaud, R. Wuthrich, Electromagnetic shielding of polymer–matrix composites with metallic nanoparticles, Composites Part B Engineering 42(6) (2011) 1420-1426.

[11] M. Jalali, T. Moliere, A. Michaud, R. Wuthrich, Multidisciplinary characterization of new shield with metallic nanoparticles for composite aircrafts, Composites Part B 50(7) (2013) 309-317.

[12] P. Saini, V. Choudhary, K.N. Sood, S.K. Dhawan, Electromagnetic interference

shielding behavior of polyaniline/graphite composites prepared by in situ emulsion pathway, Journal of Applied Polymer Science 113(5) (2010) 3146-3155.

[13] V. Panwar, J.O. Park, S.H. Park, S. Kumar, R.M. Mehra, Electrical, Dielectric, and Electromagnetic Shielding Properties of Polypropylene-Graphite Composites, Journal of Applied Polymer Science 115(3) (2010) 1306-1314.

[14] J.H. Lin, Z.I. Lin, Y.J. Pan, C.L. Huang, C.K. Chen, C.W. Lou, Polymer composites made of multi-walled carbon nanotubes and graphene nano-sheets: Effects of sandwich structures on their electromagnetic interference shielding effectiveness, Composites Part B Engineering 89 (2016) 424-431.

[15] G.T. Pham, Y.B. Park, Z. Liang, C. Zhang, B. Wang, Processing and modeling of conductive thermoplastic/carbon nanotube films for strain sensing, Composites Part B Engineering 39(1) (2008) 209-216.

[16] S. Yang, K. Lozano, A. Lomeli, H.D. Foltz, R. Jones, Electromagnetic interference shielding effectiveness of carbon nanofiber/LCP composites, Composites Part A 36(5) (2005) 691-697.

[17] J. Liang, Y. Wang, Y. Huang, Y. Ma, Z. Liu, J. Cai, C. Zhang, H. Gao, Y. Chen, Electromagnetic interference shielding of graphene/epoxy composites, Carbon 47(3) (2009) 922-925.

[18] J.-M. Thomassin, C. Jerome, T. Pardoen, C. Bailly, I. Huynen, C. Detrembleur, Polymer/carbon based composites as electromagnetic interference (EMI) shielding materials, Materials Science & Engineering R Reports 74(7) (2013) 211-232.

[19] N.C. Das, D. Khastgir, T.K. Chaki, A. Chakraborty, Electromagnetic interference shielding effectiveness of carbon black and carbon fibre filled EVA and NR based composites, Composites Part A 31(10) (2000) 1069-1081.

[20] M.H. Al-Saleh, W.H. Saadeh, U. Sundararaj, EMI shielding effectiveness of carbon based nanostructured polymeric materials: A comparative study, Carbon 60(12) (2013) 146-156.

[21] Y.-J. Chen, N.D. Dung, Y.-A. Li, M.-C. Yip, W.-K. Hsu, N.-H. Tai, Investigation of the electric conductivity and the electromagnetic interference shielding efficiency of

SWCNTs/GNS/PANI nanocomposites, Diamond and Related Materials 20(8) (2011) 1183-1187.

[22] S. Acharya, C.S. Gopinath, P. Alegaonkar, S. Datar, Enhanced microwave absorption property of Reduced Graphene Oxide (RGO)–Strontium Hexaferrite (SF)/Poly (Vinylidene) Fluoride (PVDF), Diamond and Related Materials 89 (2018) 28-34.

[23] B. Wen, X. Wang, Y. Zhang, Ultrathin and anisotropic polyvinyl butyral/Ni-graphite/short-cut carbon fibre film with high electromagnetic shielding performance, Composites Science and Technology 169 (2019) 127-134.

[24] D.D.L. Chung, Processing-structure-property relationships of continuous carbon fiber polymer-matrix composites, Materials Science & Engineering R Reports 113 (2017) 1-29.

[25] X. Zhao, J. Fu, H. Wang, The electromagnetic interference shielding performance of continuous carbon fiber composites with different arrangements, Journal of Industrial Textiles 46(1) (2015) 45-58.

[26] H.G. Kim, H.J. Shin, G.-C. Kim, H.J. Park, H.J. Moon, L.K. Kwac, Electromagnetic interference shielding characteristics for orientation angle and number of plies of carbon fiber reinforced plastic, Carbon letters 15(4) (2014) 268-276.

[27] D.D.L. Chung, A.A. Eddib, Effect of fiber lay-up configuration on the electromagnetic interference shielding effectiveness of continuous carbon fiber polymer-matrix composite, Carbon 141 (2019) 685-691.

[28] S. Geetha, K.K.S. Kumar, C.R.K. Rao, M. Vijayan, D.C.J. Trivedi, EMI Shielding: Methods and Materials-A Review, Journal of Applied Polymer Science 112(4) (2010) 2073-2086.

[29] A.A. Eddib, D.D.L. Chung, The importance of the electrical contact between specimen and testing fixture in evaluating the electromagnetic interference shielding effectiveness of carbon materials, Carbon 117(Complete) (2017) 427-436.

[30] H.C. Chen, K.C. Lee, J.H. Lin, M. Koch, Comparison of electromagnetic shielding effectiveness properties of diverse conductive textiles via various measurement

techniques, Journal of Materials Processing Technology 192(4) (2007) 549-554.
[31] C.J.V. Klemperer, D. Maharaj, Composite electromagnetic interference shielding materials for aerospace applications, Composite Structures 91(4) (2009) 467-472.
[32] D.D.L. Chung, Electromagnetic interference shielding effectiveness of carbon materials, Carbon 39(2) (2001) 279-285.
[33] Anna, Kolanowska, Dawid, Janas, P. Artur, Herman, G. Rafaa,, Auml, Drysiak, Tomasz, From blackness to invisibility: Carbon nanotubes role in the attenuation of and shielding from radio waves for stealth technology, Carbon 126 (2018) 31-25.
[34] G.S. Kumar, D. Vishnupriya, A. Joshi, S. Datar, T.U. Patro, Electromagnetic interference shielding in 1-18 GHz frequency and electrical property correlations in poly(vinylidene fluoride)-multi-walled carbon nanotube composites, Physical Chemistry Chemical Physics 17(31) (2015) 20347-20360.
[35] J. Joo, A.J. Epstein, Electromagnetic Radiation Shielding by Intrinsically Conducting Polymers, Applied Physics Letters 65(18) (1994) 2278-2280.

Chapter 3

Electromagnetic interference shielding anisotropy of unidirectional CFRP composites

3 Electromagnetic interference shielding anisotropy of unidirectional CFRP composites

3.1 Introduction

Nowadays, shielding materials play a key role in protecting electronic equipment from EMI and prevent such radiation sources from emitting radio waves. EMI shielding refers to the absorption or reflection of EM waves with efficient shielding materials, which are composed of either conductive or magnetic based materials [1, 2]. In the past few decades, metal materials have been widely used as EMI shielding materials for excellent shielding performance, but they have disadvantages of low corrosion resistance, poor mechanical flexibility, etc. [3, 4].

MXenes have been studied as EMI shielding materials due to their outstanding EMI shielding performance, low density and special metallic features [5, 6]. The MXenes composites with different structures have been fabricated to improve its EMI shielding performance [7]. Besides, carbon materials have been investigated as alternatives to metal-based composite to provide great EMI shielding performance. Polymer composites reinforced with carbon-based fillers, such as carbon fibers, graphite, carbon nanotube (CNT), graphene and carbon black have been widely studied for use as shielding materials to provide great shielding abilities to EM waves [8-14]. Conventional carbon fiber reinforced polymer (CFRP) composites show not only good

shielding properties, but also achieve excellent mechanical performance, which can expand their applications in the aeronautic industry [15-17]. Other research works [18, 19] also observed excellent shielding performance of short carbon fiber reinforced composites, but its mechanical properties and EMI shielding performance were inferior to continuous carbon fiber composite materials [20, 21]. Besides, the EMI shielding performance of CFRP could also be improved by coated with conductive paints filled with metallic particles or nanowires [22], but it still meets the challenge of poor dispersion of conductive fillers and poor wear. In recent years, intrinsically conducting polymers (ICPs) have also been used as fillers for EMI shielding [23-25], but their poor mechanical and thermal properties limit their practical applications [26].

The shielding materials should obtain excellent EMI shielding performance in the specified frequency range to meet different practical applications. Many studies have achieved the purpose of improving the EMI shielding performance of composite materials in a specific frequency band by controlling the filler's size. Jana et. al [27] found that the composite with high carbon fiber aspect ratio (L/D=100) show higher shielding effectiveness in the frequency range of 8-12 GHz (X-band). Zhao et al [28] reported that shielding performance of CFRP was enhanced with the decrease of the array spacing and the increased number of layers in the frequency range of 30-750 MHz, but the number of layers exhibited little effect on the EMI shielding of CFRP at the frequency range of 750 MHz-1.5 GHz. The shielding property of carbon nano-fiber-based composites is also improved in the X-band by increasing the magnetic particle size introduced into the matrix [29]. As above all, shielding materials with various filler

size and structures exhibits different shielding performance in various frequency band. In this chapter, EMI shielding anisotropy of unidirectional CFRP composites was investigated in the frequency range of 5-15GHz, which is often used in wireless computer networks, radar and satellite communication.

Continuous carbon fiber reinforced polymer composites have been widely used as structural materials for lightweight structures and EMI shielding applications. However, most researches have focused on the improvement of EMI shielding performance by adjusting the fiber lay-up arrangement or structure [28, 30]. Wen et al. [31] reported that the EMI SE of PVB/Ni-Gr/SCF films exhibited different performances along and perpendicular to the casting direction, where the short carbon fiber direction was changed. Hong et al. [32] indicated that the orientation of fillers could play an important role in determining EMI SE in the polymer-based composites with magnetically responsive aligned Fe_3O_4 decorated reduced graphene oxide. The previous works [31, 33] revealed that the distribution state of fillers plays an important role in the shielding performance of composites, but the shielding anisotropy didn't further be analyzed. The EMI shielding performance of CFRP composites could be influenced by the fiber orientation [34]. This chapter mainly discussed the EMI shielding anisotropy of unidirectional CFRP composites, and propose formulas to predict electrical conductivity and EMI SE of CFRP at different orientation angles.

In Chapter 2, the EMI shielding anisotropy has been proved by the transmission line method. In order to provide a theoretical analysis of shielding anisotropy of CFRP composites, a specially designed free-space measurement was set up in one direction

vibration of incident EM wave, which can measure EMI shielding performance of CFRP in any specified direction. EMI shielding anisotropy of unidirectional CFRP composites was discussed, and the theoretical formula was used to predict EMI SE of CFRP at various carbon fiber orientations. The shielding results of the free-space measurement and coaxial transmission line method were compared, and the influence of EMI shielding anisotropy on the test results with different measurements was discussed.

3.2 Experimental

3.2.1 Fabrication of unidirectional CFRP composites

The XN80 carbon fiber based unidirectional prepregs were supplied by Japan Graphite Fiber Co., Ltd. The carbon fiber areal density is 125g/m^2, and the thickness of individual prepreg is about 0.165 mm. The XN80 carbon fiber had an excellent tensile strength (3430 MPa), tensile modulus (780 GPa), electrical conductivity (5×10^{-4} ohm· cm), and the fiber diameter is about 10 μm. A four-layered unidirectional CFRP composite was made of four single prepregs arranged in the same fiber direction. The CFRP composites were cured by the hot press machine at 135 °C and 2 MPa for 1.5 h. The CFRP composite is a square with a side length of 25cm and the thickness of 0.55mm.

3.2.2 Electrical conductivity of CFRP composites

The electrical conductivity of the unidirectional CFRP composites was tested by

the four-probe method [20]. All specimens had a uniform dimension of 80 mm×10 mm×0.55 mm, and a silver paint was used to ensure good contact between the electrodes and specimens during testing. Four electrical contacts are symmetrically positioned relative to the center of the specimen, and the distance between the adjacent electrical contact is about 20mm. Each electrical contact with silver paint is 2 mm wide. A current of 0.1mA is provide by the DC power supply device (Takasago EX-375L2, Japan) at the outer electrical contacts, and the digital electrometer (Advantest R8240, USA) is used to measure the voltage at the inner contacts. Each test was carried out 5 times. Since the carbon fibers were arranged in the same direction in the unidirectional CFRPs, their ability to transfer electrons was different at various fiber orientations. The electrical conductivity of the specimens was measured at 0°, 15° 30°, 45°, 60°, 75°, and 90°. Where the 0° direction refers to the fiber direction, and 90° refers to the direction perpendicular to the carbon fiber.

3.2.3 EMI shielding measurement

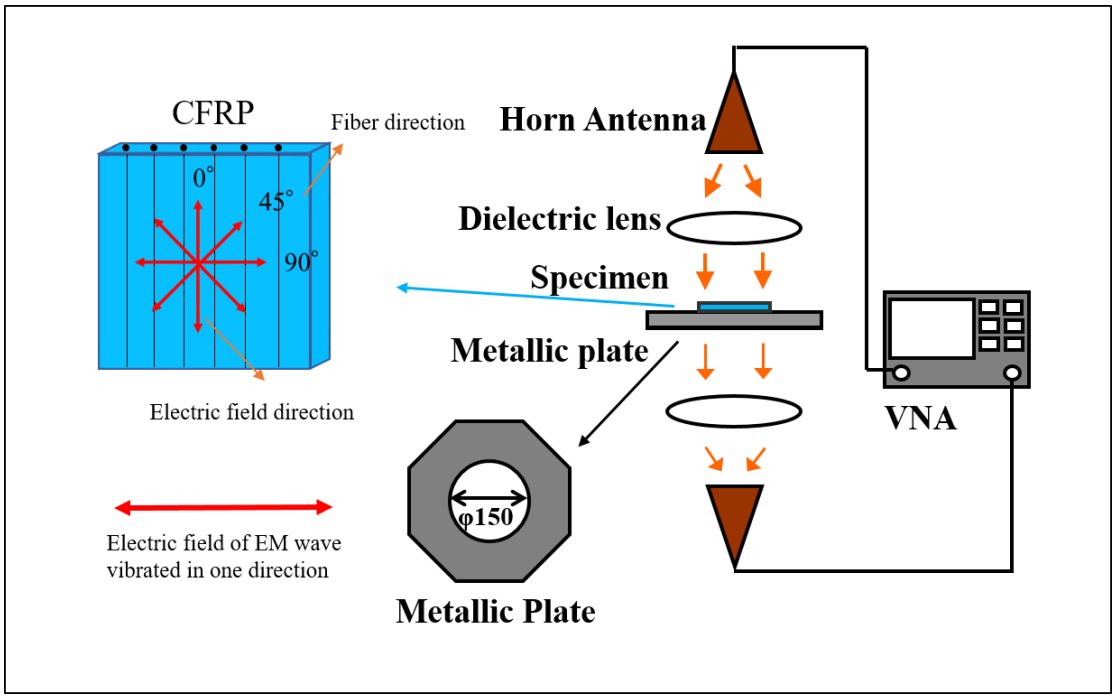

Fig. 3.1 Schematic of free-space set-up for EMI shielding measurement.

The EMI shielding performance of the CFRP composites was test by free-space measurement method coaxial transmission line measurement (Fig. 2.3). The specially designed free-space measurement system (Key-com RTS03, Japan) consists of two antennas, two lens and a sample stage as shown in Fig 3.1. The value of the scattering parameters (S_{21} or S_{12}) of the CFRP materials were tested by the vector network analyzer (Anritsu 37247D, Japan). The attenuation of the EM wave was defined as the SE, which can be calculated by the following equations:

$$SE = 10 \log\left(\frac{P_T}{P_I}\right) \quad (1)$$

$$SE = -10 \log(|S_{21}|^2) = -10 \log(|S_{12}|^2) \quad (2)$$

where P_T is the transmitted power, P_I is the incident power, and the S_{12} (S_{21}) parameters refer to the transmission coefficients.

3.3 Results and discussion

3.3.1 Electrical conductivity of unidirectional CFRP composite

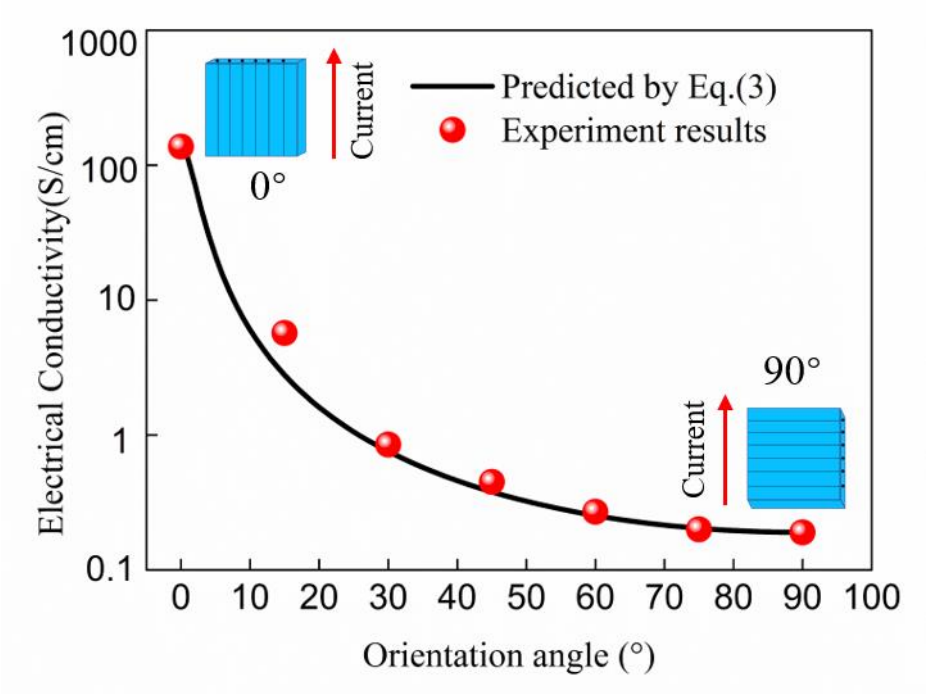

Fig. 3.2 Electrical conductivity of the CFRP at different carbon fiber orientation angles.

Fig. 3.2 shows the electrical conductivity of CFRP at the different fiber orientations of 0°, 15°, 30°, 45°, 60°, 75°and 90° (red dots). The conductivity of CFRP decreased as the fiber orientation angle increased from 0° to 90°. An anisotropic CFRP composite was described as that all the fibers are highly aligned and parallel to each other in the composite. However, the fibers are not entirely straight and have a wave shape in the composite, consequently creating many contact points between adjacent fibers. This causes the composite to have specific electrical conductivity in the transverse direction of the fiber, although it is extremely lower compared with that in the fiber direction. As consequently, the unidirectional CFRP composite shows the highest

and lowest conductivity values in the fiber direction and transverse direction, respectively.

The decreasing tendency of conductivity was not linear of CFRP decreased as the fiber orientation angle increased from 0° to 90°. The conductivity decreased sharply from 0° to around 30°, and the decreasing trend became gradual when exceeding 30°. Since the conductivity of CFRP presents a cosine change trend, the conductivity at different angles can be calculated and predicted by the formula derived below:

$$\sigma_\theta = \frac{1}{A\cos^2(\theta+\pi)+B} \quad 0 \le \theta \le \frac{\pi}{2} \tag{3}$$

where σ_θ is the electrical conductivity of CFRP at θ degree, $A=1/\sigma_0 - 1/\sigma_{90}$, $B=1/\sigma_{90}$, σ_0 and σ_{90} are the electrical conductivity of CFRP at the testing angle of 0° and 90°, respectively.

The curve in Fig. 3.2 shows the predicted electrical conductivity of unidirectional CFRP as a function of the carbon fiber orientation angle from 0° to 90°. It can be seen from Fig. 3.2 that the calculated results are in good agreement with the experimental results, indicating that the proposed formula can predict the electrical conductivity of unidirectional CFRP at any angle just through the conductivity values at 0° and 90° directions.

3.3.2 Skin depth of unidirectional CFRP composite

When the EM wave is incident on the surface of the material, the displacement current of the wave is coupled to it and generates the magnetic field at a right angle, which can create a back electromotive force to cause a force called “skin effect” [35].

As the propagation depth increase, more EM waves are attenuated. When the strength of the EM wave is reduced to 1/e of the incident strength, the distance is called the skin depth [36], and can be calculated by the following equation [37]:

$$\delta = 1/\sqrt{\pi \mu f \sigma} \quad (4)$$

Where δ is the skin depth, f is the frequency, and σ is the electrical conductivity of the material. The magnetic permeability $\mu=\mu_0\mu_r$, where the magnetic permeability of vacuum (μ_0) is $4\pi \times 10^{-7}$ H/m, and the relative magnetic permeability (μ_r) of CFRP is about 1[20, 38]

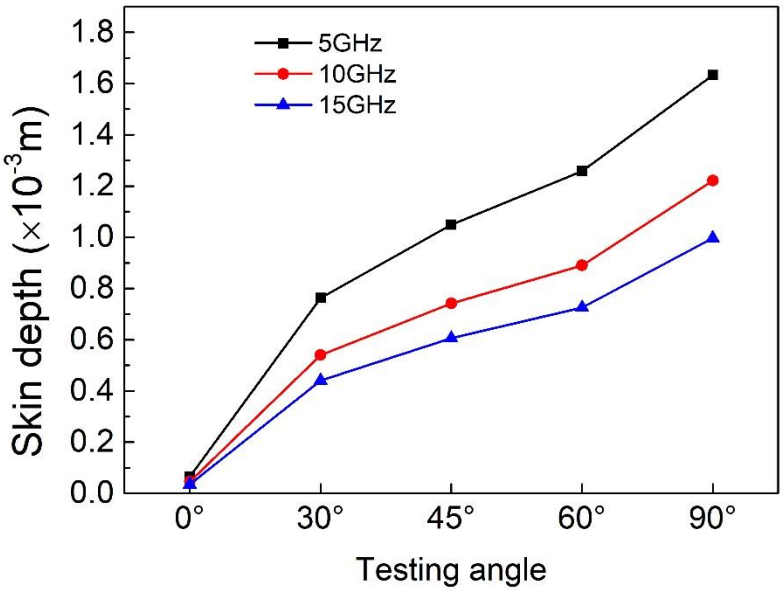

Fig. 3.3 Skin depth of CFRP as function of testing angles

Fig. 3.3 shows the skin depth of unidirectional CFRP as a function of carbon fiber orientation angles at different frequencies. The skin depth of the composite increased with an increase in the orientation angle. This is mainly due to the decrease in conductivity as the carbon fiber orientation angle increases, as shown in the conductivity results in Fig. 3.2. The skin depth also decreases as the frequency increases.

At a frequency of 15 GHz, the CFRP had the lowest skin depth value of 0.035 mm in the 0° direction, which refers to the fiber direction. At 5 GHz, CFRP obtained a maximum value of 1.633 mm in 90° direction.

The thickness of the fabricated unidirectional CFRP was about 0.55mm. According to the definition of skin depth, when the frequency is 15 GHz, and the electric field of EM wave is consistent with the fiber direction, the electric field intensity would be less than 1/e of the incident electric field intensity when the EM waves penetrate through the CFRP composite. At 5 GHz, when the electric field is perpendicular to the fiber di-rection, the electric field intensity would be greater than 1/e of the incident electric field intensity when the EM waves pass through the CFRP. Consequently, the skin depth of materials plays a key role in attenuation of EM waves, and due to the dependence of the skin depth on the carbon fiber orientation angle, the EMI shielding performance of CFRP would be different at various carbon fiber directions.

3.3.3 EMI shielding theory of CFRP composite

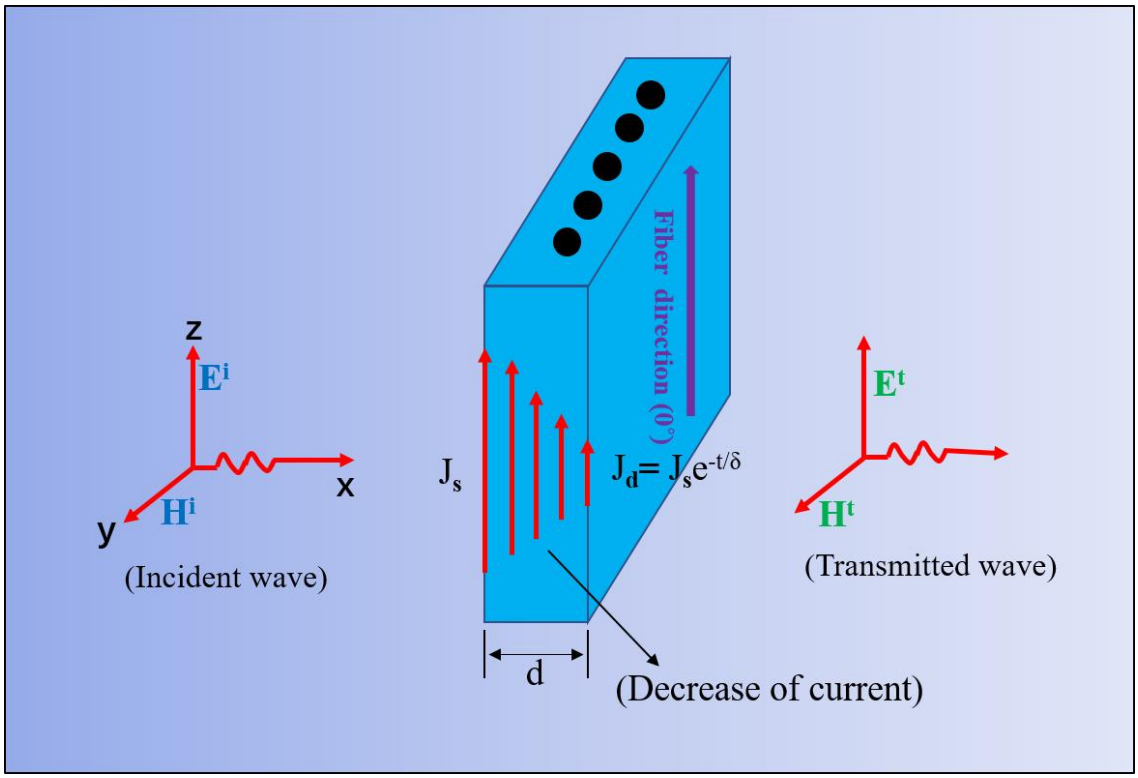

Fig. 3.4 Schematic of EMI shielding mechanism of anisotropic CFRP

According to the circuit theory [35] for calculating the EM wave attenuation by shielding, the displacement current in the wave would be coupled to the CFRP when the EM wave encounters the CFRP composite, as shown in Fig. 3.4. Then the surface current density onto the CFRP will generate a magnetic field (H) perpendicular to it, and the magnetic field would create an opposite electromotive force, which can attenuate the current to penetrate the CFRP. This phenomenon leads to the attenuation of EM waves. The shielding attenuation S(dB) for the electric field (E) can be obtained as follows:

$$S(dB) = 20\log\frac{E_I}{E_T} \quad (5)$$

$$= 20\log\frac{J_I Z_W}{J_T Z_C}$$

where E_I and E_T are the electric field at the incident side and transmitted side, respectively; J_I is the surface current density at the incident side of the CFRP, and the current value at the transmitted side J_T is expressed as:

$$J_T = J_I e^{-d/\delta} \tag{6}$$

where d is the thickness of CFRP, and δ is the skin depth.

Z_W and Z_C are the impedance of incident wave and CFRP composites, respectively, which is equal to

$$Z_W = -\frac{j377\lambda}{2\pi L}\left(L < \frac{\lambda}{2\pi}\right) \tag{7}$$

$$= 377 \ \left(L \geq \frac{\lambda}{2\pi}\right)$$

$$Z_C = \frac{1+j}{\sigma\delta(1-e^{-d/\delta})} \tag{8}$$

where σ is the electrical conductivity of the CFRP composite. Then the shielding attenuation SE (dB) of the CFRP composite can be expressed as:

$$SE(dB) = 20\log\frac{Z_W}{e^{-d/\delta}\cdot Z_C} \tag{9}$$

According to the Eq. (9), the thickness and skin depth of the material plays a decisive role in the EMI shielding performance.

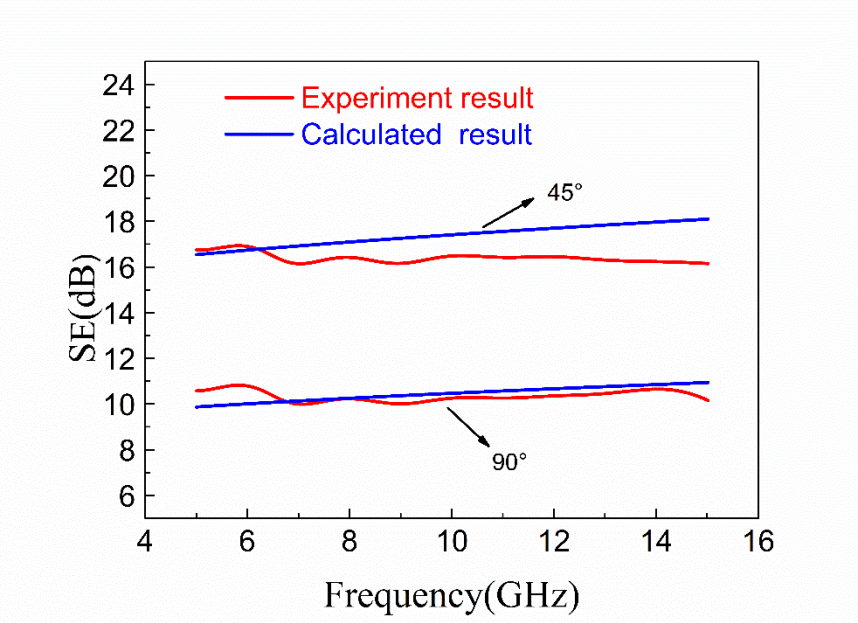

Fig. 3.5 Comparison of experimental value and formula calculation value of EMI SE

The formula's applicability in the frequency range of 5-15 GHz was verified by taking the test angles of 45° and 90° as examples. The skin depth, electrical conductivity, and related parameters were substituted into Eq. (9). The comparison between the calculated prediction and the experimental results by the free space measurement is shown in Fig 3.5. It was observed that the experimental and predicted result were in good agreement. The maximum difference at fiber orientation of 45° is only about 1.9 dB. It can be concluded that Eq. (9) can be applied to predict the EMI SE of unidirectional CFRP at the frequency range of 5 to 15 GHz.

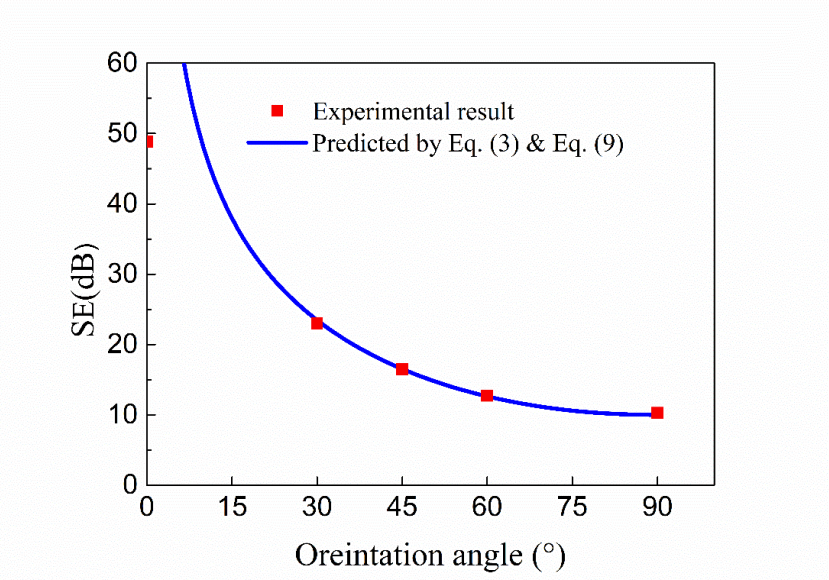

Fig. 3.6 EMI SE of CFRP for experimental and predicted results at the frequency of 10 GHz

By combining Eq. (3) and (9), EMI SE of unidirectional CFRP could be predicted at any carbon fiber orientation angles. Fig. 3.6 shows that the predicted results are highly consistent with the experimental results in the various fiber directions at 10 GHz. When only using Eq. (9) to calculate the shielding performance of CFRP at different orientation angles, it is necessary to test the material's EM parameters (skin depth, electrical conductivity, etc.) in each direction. Here, Eq. (3) and (9) are used in combination, and it is only necessary to calculate or measure the electromagnetic parameters of CFRP in the 0° and 90° directions, and substituting the results into the Eq. (9) to obtain the EMI SE at any carbon fiber orientation angles. The predicted results were highly in good agreement with the experimental values. There was a difference between the experimental and calculated results in the fiber direction (0°). That might be due to the device limitation; that is, the EMI SE of the CFRP materials might have exceeded the measuring range of the device in the fiber direction.

3.3.4 Comparison of coaxial transmission line and free-space measurement

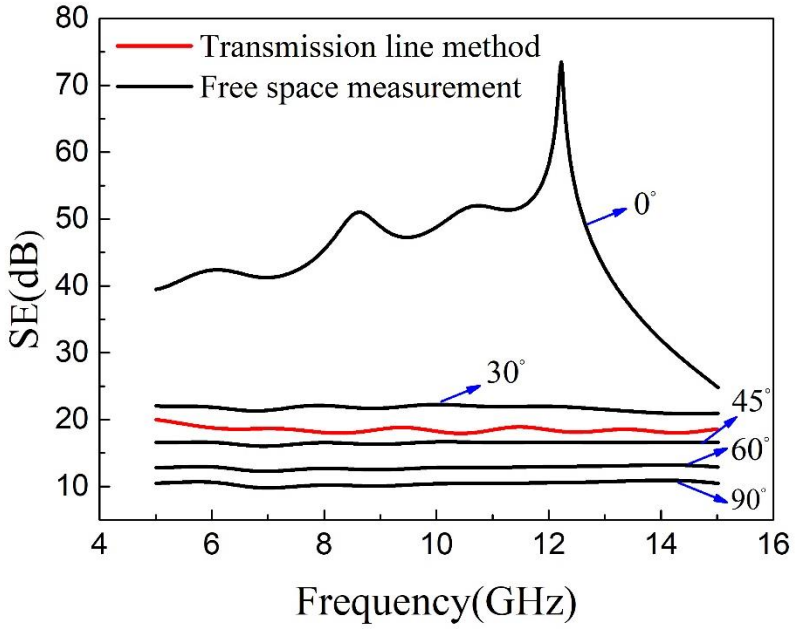

Fig. 3.7 EMI SE of CFRP by transmission line method and free-space method

To further understand the relationship between the EMI shielding performance and carbon fiber orientation, the shielding result obtained by the transmission line method was compared to that by free-space measurement. The EMI shielding perfor-mance of unidirectional CFRP with carbon fiber orientation angle of 0°, 30°, 45°, 60°, and 90° at the frequencies from 5 GHz to 15 GHz are shown in Fig. 3.7. CFRP showed an excellent EMI shielding value when the carbon fiber orientation angle is 0°, where the electric field polarization direction of EM waves is parallel to the fiber direction. The SE of CFRP decreased as the fiber orientation angle increased due to the decrease of electrical conductivity. When the orientation angle was 90°, the electric field polarization direction is perpendicular to the carbon fiber, and the CFRP obtained the lowest

electrical conductivity in this orientation angle. Thus CFRP showed the lowest SE value of about 10 dB.

The red curve in Fig. 3.8 represents the EMI shielding result measured by using coaxial transmission line method. The SE value obtained by this method was about 19 dB. This is due to the electric field of EM waves was quasi-radially distributed inside the coaxial tube (Fig. 2.3). When the coaxial transmission line method was adopted to evaluate the EMI shielding performance of unidirectional CFRP, the EMI shielding result does not change if the position of the composite material is rotated along the inner conductor. But under the free-space measurement system, the EMI shielding performance has greatly depend on the test angle. Unidirectional CFRP exhibits remarkable EMI shielding anisotropy. This characteristic of the one-side composite material can be used for the bias material of EM wave radiation, meaning that the EM waves polarized in a specific direction can be selectively shielded by adjusting the angle of the CFRP composites.

The results show that when different test methods are used to evaluate the shielding performance of unidirectional CFRP composites, the results will differ. Therefore, when assessing anisotropic materials, especially materials prepared by CFRP prepregs, special attention should be paid to the influence of EMI shielding anisotropy.

3.4 Conclusion

Carbon fiber reinforced composite materials occupy a critical position in many

structural material applications, and their EMI shielding performance has also attracted great attention. This chapter mainly investigated the EMI shielding anisotropy of unidirectional CFRP materials.

The electrical conductivity of unidirectional CFRP composites varies due to the fiber orientation angles, and the calculated results by the formulas proposed in this chapter were highly consistent with the experiment values. It is found that the skin depth of unidirectional CFRP was different at various orientation angles and frequencies. At a frequency of 15 GHz, the CFRP exhibits the lowest skin depth value of 0.035 mm in the 0° direction. All the characteristics mentioned above are key issues leading to the EMI shielding anisotropy of CFRP composites. The obvious EMI shielding anisotropy of unidirectional CFRP composites is clarified by the experimental results using specified set-up of free-space measurement. The shielding results predicted by the theoretical formula are highly consistent with the experimental results. The maximum difference between the predicted and experimental values at fiber orientation of 45° is only about 1.9 dB.

A comparison of free-space measurement and coaxial transmission line method was also conducted, and the influence of electric anisotropy on the test results was further discussed. The SE values obtained by the coaxial transmission line method was much lower than that obtained by the free-space measurement tested in the fiber direction, which indicated that special attention should be paid to the influence of the anisotropy of CFRP composites on the shielding results when evaluated by various measurements. With these results, the mechanism of EMI shielding anisotropy of CFRP

composites is clarified, which will provide an effective design of EMI shielding products with a designable shielding direction and frequency.

Reference

[1] Sankaran, S.; Deshmukh, K.; Ahamed, M. B.; Khadheer Pasha, S. K., Recent advances in electromagnetic interference shielding properties of metal and carbon filler reinforced flexible polymer composites: A review. Composites Part A: Ap-plied Science and Manufacturing 2018, 114, 49-71.

[2] Joshi, A.; Datar, S., Carbon nanostructure composite for electromagnetic interference shielding. Pramana 2015, 84, (6), 1099-1116.

[3] Abbasi, H.; Antunes, M.; Velasco, J. I., Recent advances in carbon-based polymer nanocomposites for electromagnetic interference shielding. Progress in Materials Science 2019, 103, 319-373.

[4] Ibrahim Lakin, I.; Abbas, Z.; Azis, R. S.; Abubakar Alhaji, I., Complex Permittivity and Electromagnetic Interference Shielding Effectiveness of OPEFB Fiber-Polylactic Acid Filled with Reduced Graphene Oxide. Materials (Basel) 2020, 13, (20).

[5] Wang, Z.; Cheng, Z.; Fang, C.; Hou, X.; Xie, L., Recent advances in MXenes composites for electromagnetic interference shielding and microwave absorption. Composites Part A: Applied Science and Manufacturing 2020, 136, 105956.

[6] Li, X.; Yin, X.; Liang, S.; Li, M.; Cheng, L.; Zhang, L., 2D carbide MXene Ti2CTX as a novel high-performance electro-magnetic interference shielding material. Carbon 2019, 146, 210-217.

[7] Iqbal, A.; Sambyal, P.; Koo, C. M., 2D MXenes for Electromagnetic Shielding: A Review. Advanced Functional Materials 2020, 30, (47), 2000883.

[8] Panwar, V.; Park, J.-O.; Park, S.-H.; Kumar, S.; Mehra, R. M., Electrical, dielectric, and electromagnetic shielding properties of polypropylene-graphite composites. Journal of Applied Polymer Science 2010, 115, (3), 1306-1314.

[9] Mohan, R. R.; Varma, S. J.; Faisal, M.; S, J., Polyaniline/graphene hybrid film as an

effective broadband electromagnetic shield. RSC Advances 2015, 5, (8), 5917-5923.
[10] Wu, H.-Y.; Jia, L.-C.; Yan, D.-X.; Gao, J.-f.; Zhang, X.-P.; Ren, P.-G.; Li, Z.-M., Simultaneously improved electromagnetic interference shielding and mechanical performance of segregated carbon nanotube/polypropylene composite via solid phase molding. Composites Science and Technology 2018, 156, 87-94.
[11] Hu, Y.; Li, D.; Wu, L.; Yang, J.; Jian, X.; Bin, Y., Carbon nanotube buckypaper and buckypaper/polypropylene composites for high shielding effectiveness and absorption-dominated shielding material. Composites Science and Technology 2019, 181, 107699.
[12] Bagotia, N.; Choudhary, V.; Sharma, D. K., Synergistic effect of graphene/multiwalled carbon nanotube hybrid fillers on mechanical, electrical and EMI shielding properties of polycarbonate/ethylene methyl acrylate nanocomposites. Compo-sites Part B: Engineering 2019, 159, 378-388.
[13] Wan, Y.-J.; Zhu, P.-L.; Yu, S.-H.; Sun, R.; Wong, C.-P.; Liao, W.-H., Graphene paper for exceptional EMI shielding per-formance using large-sized graphene oxide sheets and doping strategy. Carbon 2017, 122, 74-81.
[14] Zeranska-Chudek, K.; Siemion, A.; Palka, N.; Mdarhri, A.; Elaboudi, I.; Brosseau, C.; Zdrojek, M., Terahertz Shielding Properties of Carbon Black Based Polymer Nanocomposites. Materials (Basel) 2021, 14, (4).
[15] Munalli, D.; Dimitrakis, G.; Chronopoulos, D.; Greedy, S.; Long, A., Electromagnetic shielding effectiveness of carbon fibre reinforced composites. Composites Part B: Engineering 2019, 173, 106906.
[16] Yang, S.; Lozano, K.; Lomeli, A.; Foltz, H. D.; Jones, R., Electromagnetic interference shielding effectiveness of carbon nanofiber/LCP composites. Composites Part A: Applied Science and Manufacturing 2005, 36, (5), 691-697.
[17] Chung, D. D. L., Carbon materials for structural self-sensing, electromagnetic shielding and thermal interfacing. Carbon 2012, 50, (9), 3342-3353.
[18] Liang, J.-Z.; Yang, Q.-Q., Effects of carbon fiber content and size on electric conductive properties of reinforced high density polyethylene composites. Composites Part B: Engineering 2017, 114, 457-466.

[19] Chen, X.; Gu, Y.; Liang, J.; Bai, M.; Wang, S.; Li, M.; Zhang, Z., Enhanced microwave shielding effectiveness and sup-pressed reflection of chopped carbon fiber felt by electrostatic flocking of carbon fiber. Composites Part A: Applied Science and Manufacturing 2020, 139, 106099.

[20] Chung, D. D. L.; Eddib, A. A., Effect of fiber lay-up configuration on the electromagnetic interference shielding effec-tiveness of continuous carbon fiber polymer-matrix composite. Carbon 2019, 141, 685-691.

[21] Luo, X.; Chung, D., Electromagnetic interference shielding using continuous carbon-fiber carbon matrix and poly-mer-matrix composites. Composites Part B: Engineering 1999, 30, 227-231.

[22] Dupenne, D.; Lonjon, A.; Dantras, E.; Pierre, T.; Lubineau, M.; Lacabanne, C., Carbon fiber reinforced polymer metalli-zation via a conductive silver nanowires polyurethane coating for electromagnetic shielding. Journal of Applied Polymer Science 2020, 138, (14), 50146.

[23] Kumar, V.; Muflikhun, M. A.; Yokozeki, T., Improved environmental stability, electrical and EMI shielding properties of vapor-grown carbon fiber-filled polyaniline-based nanocomposite. Polymer Engineering & Science 2018, 59, (5), 956-963.

[24] Yin, G.; Wang, Y.; Wang, W.; Yu, D., Multilayer structured PANI/MXene/CF fabric for electromagnetic interference shielding constructed by layer-by-layer strategy. Colloids and Surfaces A: Physicochemical and Engineering Aspects 2020, 601, 125047.

[25] Yokozeki, T.; Goto, T.; Takahashi, T.; Qian, D.; Itou, S.; Hirano, Y.; Ishida, Y.; Ishibashi, M.; Ogasawara, T., Development and characterization of CFRP using a polyaniline-based conductive thermoset matrix. Composites Science and Technology 2015, 117, 277-281.

[26] Gupta, S.; Tai, N.-H., Carbon materials and their composites for electromagnetic interference shielding effectiveness in X-band. Carbon 2019, 152, 159-187.

[27] Jana, P. B.; Mallick, A. K.; De, S. K., Effects of sample thickness and fiber aspect ratio on EMI shielding effectiveness of carbon fiber filled polychloroprene composites in the X-band frequency range. IEEE Transactions on Electromagnetic Compatibility

1994, 34, (4), 478-481.

[28] Zhao, X.; Fu, J.; Wang, H., The electromagnetic interference shielding performance of continuous carbon fiber composites with different arrangements. Journal of Industrial Textiles 2015, 46, (1), 45-58.

[29] Bayat, M.; Yang, H.; Ko, F., Effect of iron oxide nanoparticle size on electromagnetic properties of composite nanofibers. Journal of Composite Materials 2017, 52, (13), 1723-1736.

[30] Hassan, A. M.; Douglas, J. F.; Garboczi, E. J., Computational modeling of the electromagnetic characteristics of carbon fiber-reinforced polymer composites with different weave structures. 2014, 1494-1499.

[31] Wen, B.; Wang, X.; Zhang, Y., Ultrathin and anisotropic polyvinyl butyral/Ni-graphite/short-cut carbon fibre film with high electromagnetic shielding performance. Composites Science and Technology 2019, 169, 127-134.

[32] Hong, S. Y.; Kim, Y. C.; Wang, M.; Nam, J.-D.; Suhr, J., Anisotropic electromagnetic interference shielding properties of polymer-based composites with magnetically-responsive aligned Fe3O4 decorated reduced graphene oxide. European Polymer Journal 2020, 127, 109595.

[33] Xu, Y.; Yang, Y.; Yan, D.; Duan, H.; Dong, C.; Zhao, G.; Liu, Y., Anisotropically conductive polypropylene/nickel coated glass fiber composite via magnetic field inducement. Journal of Materials Science: Materials in Electronics 2017, 28, (12), 9126-9131.

[34] Ni, Q-Q.; Inoue, M.; Zhang, L., Electromagnetic shielding property of CFRP composite laminates, 18th International Conference on Composites Materials (ICCM), ICCM18, Jeyu Island, Korea, 2011

[35] Kunke, G. M., Shielding of Electromagnetic Waves. Springer Switzerland, 2020.

[36] Liu, X.; Yin, X.; Kong, L.; Li, Q.; Liu, Y.; Duan, W.; Zhang, L.; Cheng, L., Fabrication and electromagnetic interference shielding effectiveness of carbon nanotube reinforced carbon fiber/pyrolytic carbon composites. Carbon 2014, 68, 501-510.

[37] Paul, C. R., Introduction to electromagnetic compatibility. John Wiley & Sons, Inc.,: New Hersey, 2006.

[38] Karbhari, V. M., Non-Destructive Evaluation (NDE) of Polymer Matrix Composites. Woodhead Publishing Limited: Sawston, Cambridge, UK, 2013.

Chapter 4

✵✵✵✵✵✵✵✵✵✵✵✵✵✵✵✵✵✵✵✵✵✵✵✵✵✵✵✵

Damage detection of CFRP composites by electromagnetic wave nondestructive testing (EMW-NDT)

✵✵✵✵✵✵✵✵✵✵✵✵✵✵✵✵✵✵✵✵✵✵✵✵✵✵✵✵

4 Damage detection of CFRP composites by electromagnetic wave nondestructive testing (EMW-NDT)

4.1 Introduction

Carbon-based composites have been widely used in various industries [1-3] due to their high mechanical and electrical performances [4, 5]. Specifically, carbon fiber reinforced polymer (CFRP) composites have been widely used to replace high-density metal materials [6, 7], due to their high elastic modulus and strength to weight ratio as well as their excellent corrosion resistance. The application of CFRP include aircraft, wind turbines, automobiles, and sports items such as bicycles, skis, and rowing boats [8]. With the diversification of CFRP applications, its production process has become fairly complicated. Many defects and damages will appear in the production and application processes. For example, unevenness of resins and appearance of voids will occur during the production process, and the material will crack and delaminate after being impacted in the application process [9, 10]. The presence of these defects will significantly affect the performance and application of the CFRP materials, with the delamination and crack damage in the composite materials particularly difficult to detect, leading to hidden safety hazards during use. Therefore, carrying out nondestructive testing (NDT) is essential to evaluate the various damage to CFRPs during their production and service.

A number of NDT methods currently exist for detecting the defects and damage within composite materials. Among them, the eddy current testing method has been extensively studied. This is a noncontact method mainly used to detect cracks and corrosion in high conductivity materials [11, 12]. To improve the damage detection in CFRPs, Wu et al. developed a T-R probe with a special structure, to overcome the impact of lift-off variation and detected the defects within CFRPs [13]. A novel wireless power transfer-based eddy current NDT using a flexible printed coil array has been proposed by L. U. Daura et al. [14], which can be used for the eddy current testing (ECT) of pipeline sample. Elsewhere, Mizukami et al. designed and changed the probe geometry of the eddy current testing setup to improve the sensitivity to delamination in CFRPs, with a delamination with a length and width of 10 mm consequently observable [15]. Meanwhile, He et al. found that the defects induced by a low-energy impact can be effectively detected via scanning pulsed eddy current testing [16]. Many researchers also studied the application of eddy current testing in CFRP examination through modeling [17, 18]. Due to the electrical performance requirements in the eddy current testing method, the method is not mature in the terms of CFRP testing. At the same time, the method also exhibits certain other disadvantages, such as the limitation of the penetration depth and the unsuitability for the detection of complex geometries and large area products.

Another prevalent and widely used NDT method is the ultrasonic testing method, which has mainly been used to detect material delamination. The ultrasonic C-scan technique can identify the location, orientation, and size of defects. Many research

reports demonstrated the use of ultrasonic NDT for the detection of impact damage in CFRPs [19-21]. However, a number of disadvantages remain in using the ultrasonic NDT method. For example, a medium is required to transmit ultrasonic energy from the probe to the material, such as water and gel, and detecting the delamination that exists near the surface of the material is not easy [15, 22]. While a relatively new ultrasonic NDT has been developed which involves noncontact without the requirement of a coupling medium, the method exhibits many limitations and must be performed under specific conditions [23, 24].

Meanwhile, in terms of other methods, while shearography [25, 26] and radiographic testing [27, 28] methods have been applied to the examination of CFRP materials, these also involve certain limitations, such as being only applicable to the detection of particular specimens and being limited to certain types of damage [29]. The infrared thermography method can be used to detect defects through monitoring the temperature variations caused by the discontinues in the material [30]. R. Sutthaweekul et al. [31] proposed a novel application of microwave NDT to detect and characterize the flat-bottom hole (FBH) defect in coated glass fiber reinforced plastics (GFRP) pipes. Numerous works [32-34] focused on the application of thermal imaging technology in relation to composites, with the cost of the machine and the hot spots where reflective surfaces are prone to error found to limit its full application.

Free-space measurement is generally used to determine the magnetic permeability and electric permittivity of materials and can be conducted under different temperature conditions [35, 36]. A number of research works demonstrated the possibility of

applying a free-space method, to detect hardened cement specimens [37] and to determine the dispersion and orientation of the fiber that exists in concrete [38]. However, few reports focused on the application of the EM wave technique as a nondestructive testing of CFRP for evaluate CFRP damage.

Due to the high electrical conductivity of carbon fiber, CFRPs always achieve an excellent electromagnetic interference (EMI) shielding performance. When a damage occurs inside CFRP composites, the single-layer composite material will become a regional “double-layer” or “multi-layer” material, where the air layer is formed. Multiple reflections will occur when the EM wave passes through these regions, resulting in changes to the transmission coefficient. The damage inside the CFRP could be detected through analyzing and comparing the difference in transmission coefficient. In this chapter, a new type of NDT method using electromagnetic wave (EMW-NDT) is proposed to detect the damage in CFRP composites. The inspection ability of this method in relation to the different types of damages inside CFRP composites is investigated. The EMW-NDT present a noncontact and nondestructive measurement method, wherein a coupling medium is not required. This method allows for testing samples of large sizes with various shapes, and the test process is quick where the testing results could be obtained in few seconds. As the electrical conductivity of CFRP was affected by the carbon fiber direction [39, 40], the detection performance of the EM wave technique at the different angles of incident EM wave between the electric field of the EM waves and carbon fiber direction was analyzed. The experimental results indicated that the proposed EMW-NDT method is effective in detecting damage

such as delamination, crack or other defects in CFRP composites.

4. 2 Experiments

4.2.1 Sample preparation

The CFRP samples were fabricated from unidirectional prepreg sheets. The delamination damage was reproduced by inserting Teflon film between the CFRP layers. The main reason for choosing Teflon film is its high electrical resistance (almost insulation) and dielectric constant value (≈2.1), which is close to that of air (≈1). Slits in the CFRPs were prepared using a knife. The sample dimension was 250 mm in length and 250 mm in width. All the CFRP composites were cured using a hot press machine at 135°C, 2 MPa for 1.5 hours, as shown in Fig. 4.1.

Carbon prepregs sheets (NT81250-525S) with an areal density of 125g/m^2 were supplied by Nippon Graphite Fiber Corporation, while the Teflon film was purchased from Nitto Denko Corporation, with the intrinsic properties listed in Table 4.1.

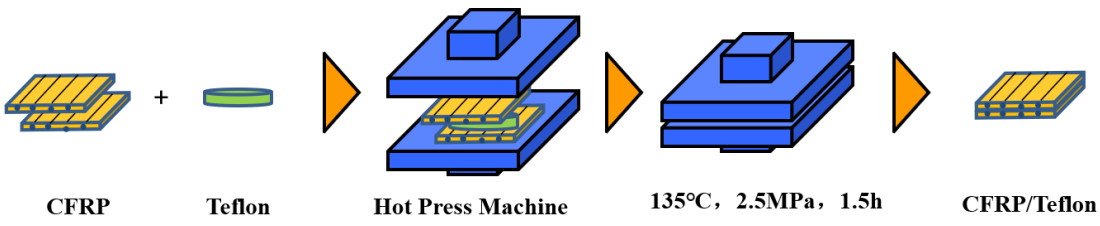

Fig. 4.1 Fabrication process of CFRP composites inserted with Teflon film.

Table 4.1 Properties of the Teflon film

Profile	Unit	Value
Thickness	0.05	mm
Permittivity	2.1	-
Volume Resistivity	over 1×10^{17}	Ω•cm

4.2.2 EMW-NDT measurement

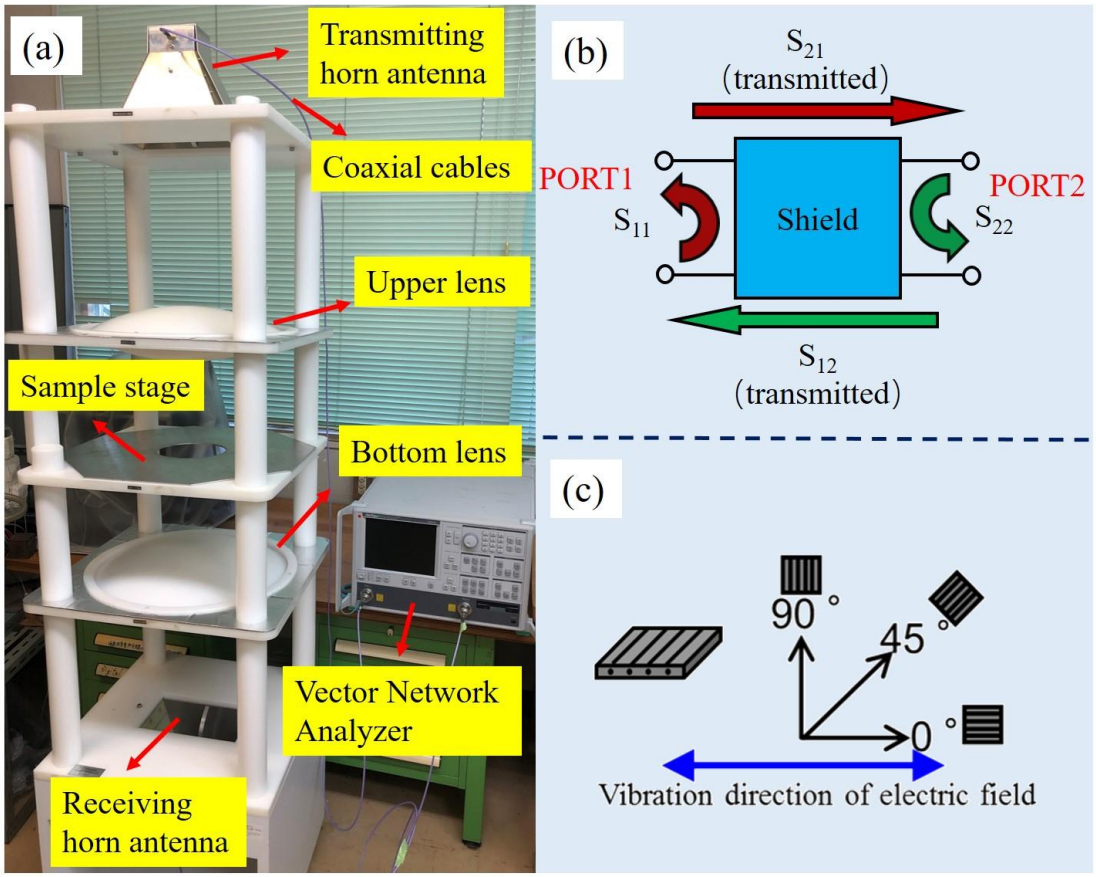

Fig. 4.2 (a) The specially designed free-space measurement system and its set-up, (b) illustration of the S-parameter obtained via measurement, (c) incident angle of the EM wave between fiber direction and electric field direction.

To measure the changes in electromagnetic performance for detecting damages inside the CFRP, the electric field of the incident EM waves was linearly polarized. As shown in Fig. 4.2(a), the free-space setup consisted of transmitting and receiving horn antennas connected to a vector network analyzer by two coaxial cables. A pair of dielectric lenses was mounted between the transmitting and receiving antennas. The upper lenses demonstrated the capacity to convert the spherical EM wave emitted by the transmitting antenna into a linearly polarized plane wave. After the sample shielded the EM wave, the remaining EM waves were converted and focused by the bottom lens,

and the converging beam ultimately reached the receiving antenna. The presence of the lens reduced the multiple reflections between the transmitting antenna and the sample as well as the diffraction around the sample, which significantly improved the accuracy of the test results.

A sample stage between the two antennas was present, which was used for the placement of the sample during the test. Since the free-space setup was placed vertically, no fixture was required to secure it. An aperture was used in the middle of the sample stage, with the measured part of the sample placed within the aperture range. We prepared sample stage with aperture diameters of 16 cm. To avoid the impact of edge effects and multiple reflections, the device was required to be calibrated prior to the measurement. The maximum size of specimen that can be tested by this method depends on the sample stage size, the distance between antennas, and other related parameters. The device could be suitable for the detection of large-size composite structures through proper modification.

The transmission scatter parameters (S_{21}) (Fig. 4.2(b)) was recorded by the vector network analyzer at the frequency range of 5-15 GHz. The attenuation of the EM wave was defined as the shielding effectiveness (SE), which could be calculated using the following equations:

$$SE = S_{21}(dB) = -10\log(|S_{21}|^2) \quad (1)$$

while the detection sensitivity ΔS_{21}(dB) can be defined as follows:

$$\Delta S_{21}(dB) = S'_{21}(dB) - S_{21}(dB) \quad (2)$$

where S'_{21}(dB) and S_{21}(dB) are the transmission coefficient of CFRP with and without

delamination damage, respectively.

The electrical conductivity of CFRP is affected by the direction of the carbon fiber, i.e., the angle between the fiber direction and the electric field direction of the incident EM wave will affect the transmission coefficient. To ascertain the optimum incident angle of the EM wave for the best detection sensitivity of damage within CFRPs, the samples were evaluated using three typical incident angles of 0°, 45° and 90° as shown in Fig. 4.2(c).

4.3 Results and discussions

4.3.1 Electromagnetic interference shielding theory

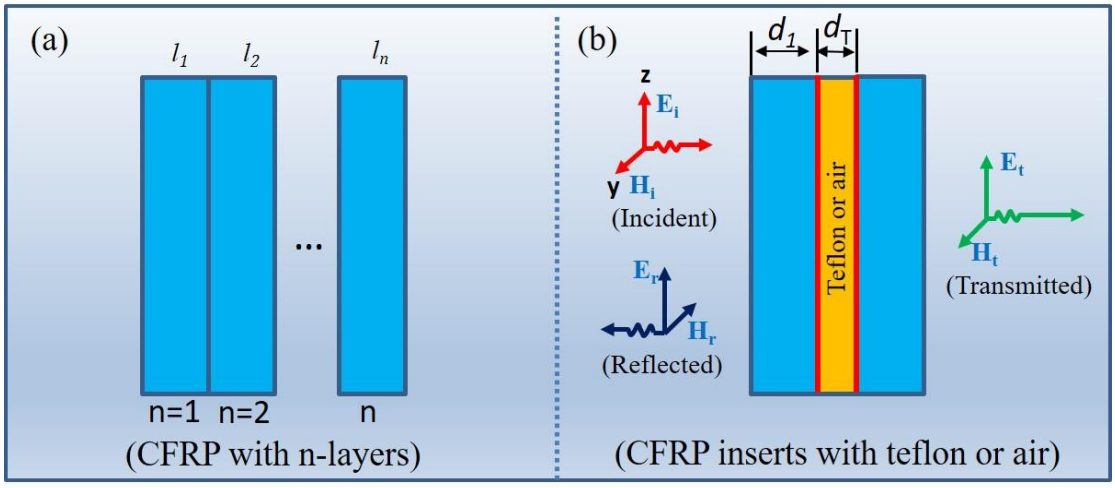

Fig. 4.3. CFRP with different structures: (a) n-layers CFRP; (b) CFRP separated by Teflon film or air.

According to the multimedia shielding theory [41], the transmission coefficient T of n-layer materials (Fig. 4.3(a)) for the H-field is:

$$T = p[(1 - q_1 e^{-2r_1 l_1})(1 - q_2 e^{-2r_2 l_2}) \cdots (1 - q_n e^{-2r_n l_n})]^{-1} \times e^{-r_1 l_1 - r_2 l_2 \cdots - r_n l_n} \quad (3)$$

Meanwhile, the total shielding SE_T, absorption SE_A, reflection SE_R, and the multiple reflection SE_M are expressed as follows:

$$SE_T = SE_A + SE_R + SE_M = 20log_{10}|T| \quad (4)$$

$$SE_A = 20log_{10}\left|e^{-r_1 l_1 - r_2 l_2 \cdots - r_n l_n}\right| \quad (5)$$

$$SE_R = 20log_{10}|P| = 20log\left|\frac{2\eta_0 \cdot 2\eta_1 \cdot\cdot 2\eta_n}{(Z_w+\eta_1)(\eta_1+\eta_2)\cdot\cdot(\eta_n+Z_w)}\right| \quad (6)$$

$$SE_M = 20log_{10}[(1 - q_1 e^{-2r_1 l_1})(1 - q_2 e^{-2r_2 l_2}) \cdots (1 - q_n e^{-2r_n l_n})]^{-1} \quad (7)$$

where q is the reflection coefficient, p is the transmitted coefficient, l is the shield thickness, η is the intrinsic impedance of the shield, Z_W is the EM wave impedance, and r is the propagation constant.

$$r = \sqrt{j\omega\mu(\sigma + j\omega\varepsilon)} \quad (8)$$

$$q_n = \frac{(\eta_n - \eta_{n-1})(\eta_n - Z_W)}{(\eta_n + \eta_{n-1})(\eta_n + Z_W)} \quad (9)$$

For a single layer CFRP with thickness d and intrinsic impedance Z_B, the total shielding effectiveness (SE_S) can be expressed as follows:

$$\begin{aligned} SE_S &= 20log_{10}|T| \quad (10)\\ &= SE_A + SE_R + SE_M \\ &= 20log_{10}(e^{-rd}) + 20log\left|\frac{2Z_W \cdot 2Z_B}{(Z_W+Z_B)(Z_B+Z_w)}\right| + 20log|1 - qe^{-2rd}| \\ &= 8.68\frac{d}{\delta} + 20\log_{10}\frac{|K+1|^2}{4|K|} + 20\log_{10}\left|1 - \frac{(K-1)^2}{(K+1)^2}e^{-2rd}\right| \end{aligned}$$

where k is the ratio between the EM wave impedance (Z_W) and intrinsic impedance (Z_B) of CFRP, while δ is the skin depth, as below:

$$\delta = 1/\sqrt{\pi\mu f\sigma} \quad (11)$$

Where μ is magnetic permeability, f is frequency, and σ is electrical conductivity.

For a CFRP with Teflon or air inserts (Fig. 4.3(b)), it will be imaged as a multi-

layer structure with n=3, with the thickness d_1, half that of single CFRP (d). The thickness of Teflon or air are d_T. According to Eq. (4), the SE value of CFRP with Teflon film or air (SE_d) can be rewritten follows:

$$SE_d = 20log_{10}\left(e^{-rd_1 - r_t d_T - rd_1}\right) + 20log\left|\frac{2Z_w \cdot 2Z_B \cdot 2Z_T \cdot 2Z_B}{(Z_w + Z_B)(Z_B + Z_T)(Z_T + Z_B)(Z_B + Z_w)}\right| + 20log\left|\left(1 - q_1 e^{-2r_1 d_1}\right)\left(-q_2 e^{-2r_2 d_T}\right)\left(-q_3 e^{-2r_1 d_1}\right)\right|$$

$$= 8.68\frac{d_1 + d_2}{\delta} + 20\log_{10}\frac{|K+1|^2}{4|K|} + 20\log_{10}\frac{|K_1+1|^2}{4|K_1|} + 20log\left|(1 - q_1 e^{-2r_1 d_1})(-q_2 e^{-2r_2 d_T})(-q_3 e^{-2r_1 d_1})\right| \quad (12)$$

To discuss the effect of Teflon/air on the EMI shielding performance of CFRP, we compared the SE value of CFRP with/without Teflon/air. Here, the detection sensitivity, ΔS_{21}(dB), could be expressed as follows:

$$\Delta S_{21}(dB) = SE_d - SE_s \quad (13)$$

$$= 20\log_{10}\frac{|K_1+1|^2}{4|K_1|} + 20log\left|(1 - q_2 e^{-2r_2 d_T})\right| \text{ , } K_1 = Z_T/Z_B$$

Here, $K_1 = Z_T/Z_B$, and if the Teflon was replaced by the air, the formula will change to as follow:

$$\Delta SE_a = SE_a - SE_s \quad (14)$$

$$= 20\log_{10}\frac{|K+1|^2}{4|K|} + 20log\left|(-q_2 e^{-2r_2 d_T})\right| \text{ , } k = Z_W/Z_B$$

where Z_T is the impedance of Teflon or air.

Here, $d=0.55\times10^{-3}$m, $d_1=d_2=d/2=0.275\times10^{-3}$m, and the electrical conductivity σ of CFRP at the test degree 45° was 453 S/m. Then, the detection sensitivity ΔS_{21}(dB) for the CFRP with Teflon and air at 10GHz were 4.6 and 5.7 dB. This indicated that the

insertion of Teflon film in CFRP can improve the shielding performance of the material, which means that the delamination damage inside the CFRP could be detected by comparing the transmission coefficient value changes. Simultaneously, the theoretical analysis results also indicated that the EMI shielding effectiveness was similar to that of the CFRP inserted with air or Teflon film.

4.3.2 Detection sensitivity of delamination damage size by ΔS_{21} (dB)

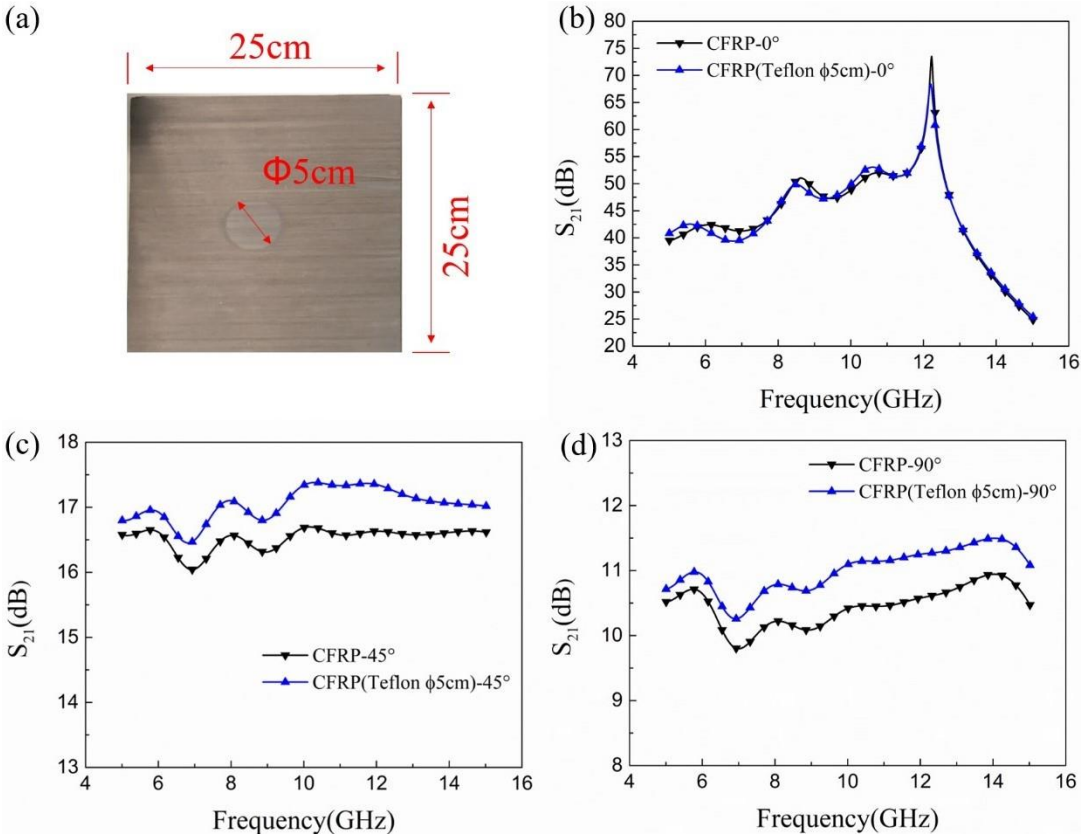

Fig. 4.4 (a) Images of CFRP inserts of Teflon with different diameters; S_{21}(dB) values of CFRPs inserted with 5 cm diameter Teflon film under three typical incident angles of (b) 0°, (c) 45° and (d) 90°

Table 4.2 Skin depth and detection sensitivity ΔS_{21}(dB) of CFRPs with different incident angles at 10 GHz

Incident angle of EM wave	0°	45°	90°
Skin depth δ (mm)	0.0459	0.742	1.221
Detection sensitivity (dB)	0.46	0.78	0.67

To accurately predict the service life of CFRPs, the ability to quantitatively characterize any delamination defects via NDT technology is essential. The delamination size is a main factor affecting the CFRP's service life, meaning detecting the delamination area is critical in the NDT process. The CFRP with delamination areas of Φ 5cm in diameter was reproduced by inserting Teflon film. The samples were square shaped with a side length of 25 cm, as shown in Fig. 4.4(a), with the measurement involving the sample stage of a Φ16 cm diameter aperture.

Fig. 4.4(b) shows the S_{21}(dB) values of CFRP at the incident angle of 0°. With the change in Teflon area inside the CFRP, the S_{21}(dB) value changed at specific frequencies; however, the differences in S_{21}(dB) were not large enough to distinguish the delamination area. Fig. 4.4(c) and (d) show the S_{21}(dB) values of the CFRP at the testing angle of 45° and 90°, respectively. A detectable difference in S_{21}(dB) values was obtained within the entire frequency range of 5-15 GHz. Here, it was clear that the existence of delamination led to an increase in the SE values of the CFRP. Then, with the delamination damage created inside the CFRP composites, the single-layer CFRP composite was split into a “double-layer” version, and the air zone was formed. Multiple reflections would occur when the EM wave passed through these regions, resulting in the improvement of the EMI shielding performance, which was consistent with the shielding theory analyzed in the previous section.

The variation in SE value is shown in Table 4.2. The lower detection sensitivity of delamination at the 0° incident angle was deemed to be due to the small skin depth for CFRP at the fiber direction. Eq. (11) indicates that the skin depth decreases with the

increase in frequency and electrical conductivity. Due to the anisotropy of the electrical conductivity of unidirectional CFRP, this material exhibits the highest electrical conductivity at the fiber direction, resulting in the smallest skin depth. For example, the skin depth of CFRP at 10 GHz was around 0.0459 mm in the fiber direction (0°), as shown in Table 4.2. According to the definition of skin depth, at a 0° incident angle where the electric filed is consistent with the fiber direction, the EM wave strength would be reduced to 1/e of its incident strength before the EM wave is transmitted out the CFRP composites. That is, most of the EM wave cannot reach the depth of the delamination area, resulting in a small detection sensitivity. At the 10 GHz frequency, the skin depth was calculated to be 0.742 mm at the 45° incident angle and 1.221 mm at the direction perpendicular to the carbon fiber (90°), which are far larger than its thickness (0.55 mm). Consequently, the penetration ability of the EM wave to the CFRP was improved as the incident angle testing angle to fiber orientation increased, and the delamination size was detected at the incident angles of 45° and 90°, which is shown in Fig. 4.4(c) and Fig. 4.4(d). Here, the delamination area ratio is about 9.8%, then the detection sensitivity of the damage area ratio was around 12.6%/dB at the 45° incident angle.

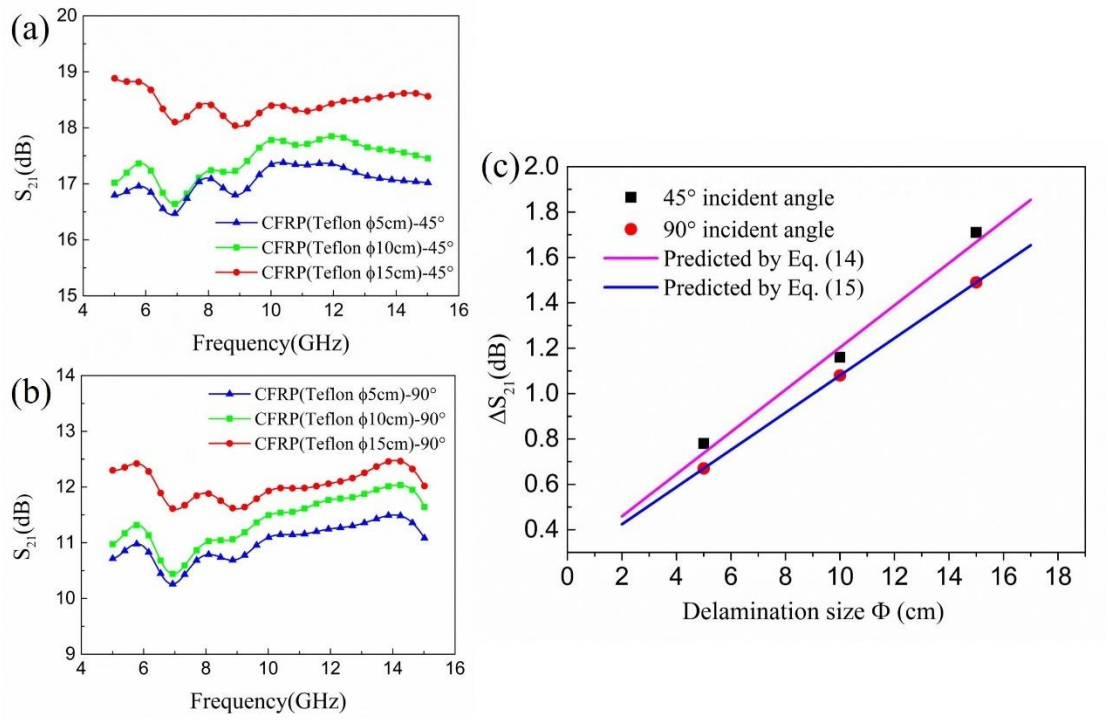

Fig. 4.5. (a) (b) S_{21}(dB) values of CFRPs inserted with various diameters of Teflon film under the testing angles of 45° and 90°; (c) detection sensitivity at 10 GHz;

The influence of delamination size on the detection sensitivity was investigated by changing the delamination areas reproduced by inserting Teflon films with different diameters (Φ5, Φ10 and Φ15cm). These were remarked as CFRP (Teflon Φ5cm), CFRP (Teflon Φ10cm) and CFRP (Teflon Φ15cm), and they exhibited delamination areas of 9.8%, 39% and 87.9%, respectively. Fig. 4.5(a) and Fig. 4.5(b) show the relationship between the variation in SE value and the delamination area at the incident angles of 45° and 90°, respectively. The greater the delamination areas, the more EM waves were attenuated due to the delamination damage in the CFRP composites. This means that the delamination size could be detected using the proposed EMW-NDT method.

As Fig. 4.5(c) shows the detection sensitivity value increased with the increment of the delamination size. The detection ability at the 45° incident angle is better than that at the 90° angle. The detection sensitivity of the delamination area at the 45° and

90° can be predicted approximately as follows:

ΔS_{21} (dB)=0.093×d+0.27 for the 45° incident angle (14)

ΔS_{21} (dB)=0.082×d+0.26 for the 90° incident angle (15)

The predicted results are in good consistent with the experimental, as shown in Fig. 4.5(c), which means the diameter of delamination area could be predicted by the above formulas.

4.3.3 Detection sensitivity of delamination thickness by ΔS_{21} (dB)

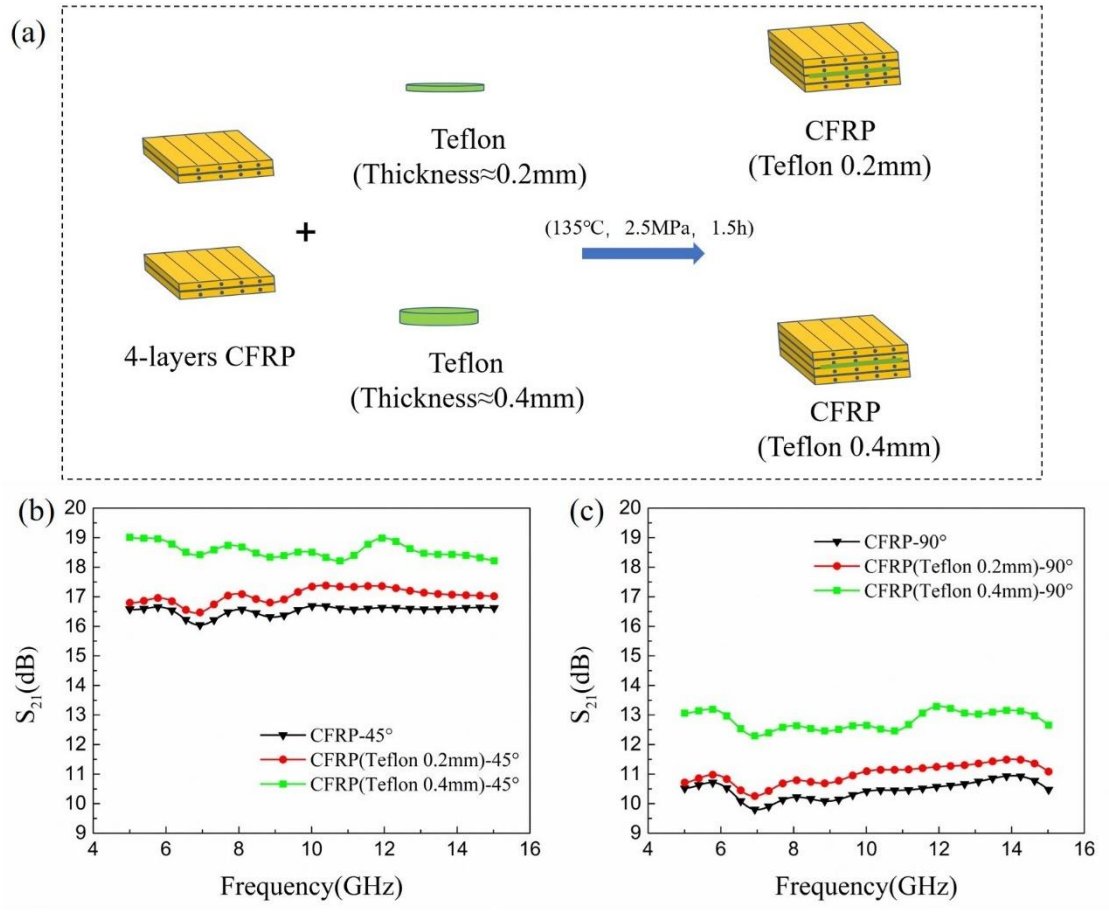

Fig. 6. (a) Preparation process of CFRP inserted with different thicknesses of Teflon film; (b) (c) SE values at the incident angles of 45° and 90°.

Table 4.3 Detection sensitivity ΔS_{21} (dB) of delamination thickness at 10 GHz

Specimen	45° testing angle		90° testing angle	
	S_{21}(dB)	ΔS_{21} (dB)	S_{21}(dB)	ΔS_{21} (dB)
CFRP	16.68	/	10.41	/
CFRP (Teflon 0.2 mm)	17.34	0.66 dB	11.09	0.69 dB
CFRP (Teflon 0.4 mm)	18.5	1.82 dB	12.64	2.23 dB

The delamination thickness is another critical quantitative index for evaluating the damage and service life of CFRP composites. Fig. 4.6(a) shows the fabrication process of the CFRPs with different delamination thicknesses, which were reproduced using the insertion of 0.2 mm and 0.4 mm thick Teflon films.

As discussed in the previous section, the lower detection sensitivity at the fiber direction was mainly due to the smaller skin depth and poor transmit ability of the EM wave at the 0° incident angle, and thus, the detection sensitivity to the delamination thickness was investigated at the incident angles of 45° and 90°. A clear difference in SE value could be observed in the entire frequency range of 5-15 GHz as shown in Fig. 4.6(b) and Fig. 4.6(c), where the SE value increased with the increment in delamination thickness. The largest detection sensitivity of the CFRP with a 0.4 mm delamination thickness was 2.23 dB as shown in Table 4.3, which means the sensitivity of the thickness change was around 5.6 dB/mm. Thus, it can be concluded that the delamination thickness inside CFRPs can be identified successfully by the EMW-NDT method at an incident angle of 45° and/or 90°.

4.3.4 Detection of crack damage

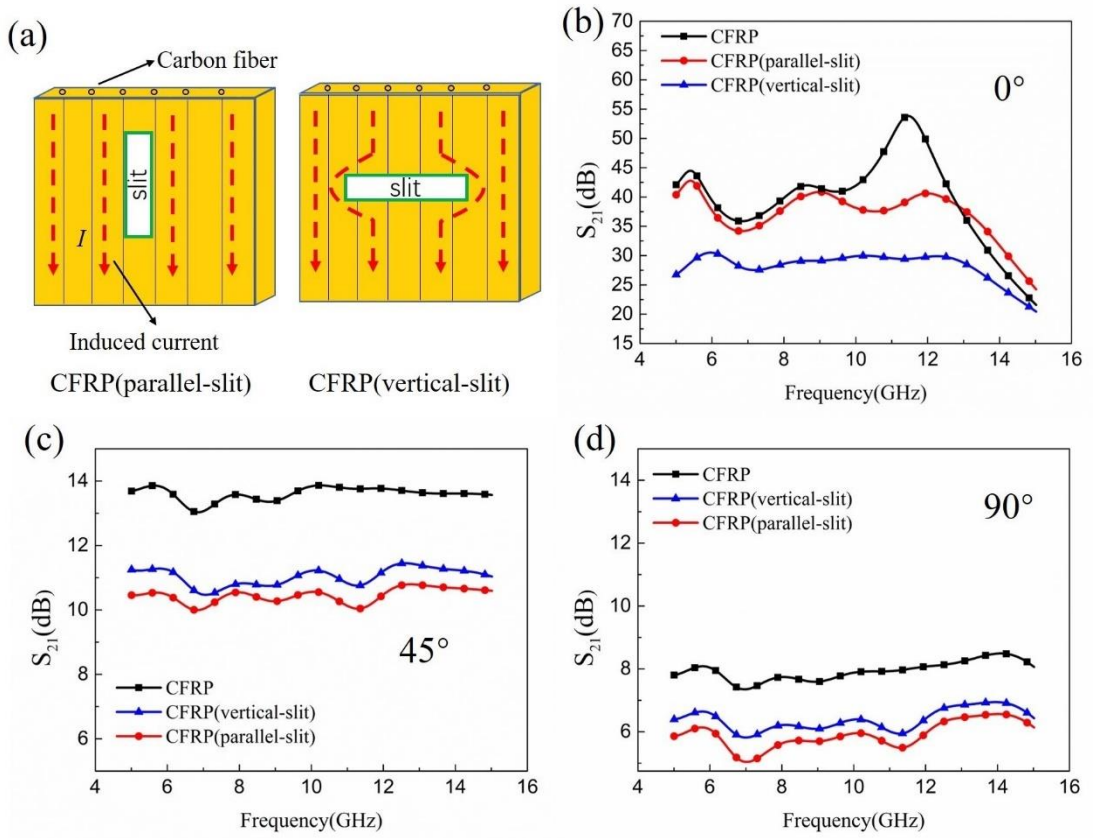

Fig. 4.7 (a) CFRPs with slits; SE values of the CFRPs at different incident angles of (b) 0°, (c) 45°, and (d) 90°

To investigate crack damage, a slit was reproduced in the unidirectional CFRP samples. Two types of slit, one vertical and one parallel to the fiber direction, were introduced. Fig. 4.7(a) shows the SE results for the two slits. When EM waves penetrate into CFRP composites, the displacement current will be coupled to the surface of the CFRP to create a magnetic field perpendicular to the current, as shown in Fig. 4.7(a). An electromotive force running opposite to the induced current is then formed, which is known as the "skin effect" [42]. The EM waves will be attenuated by this skin effect when penetrate through the CFRP composites. Therefore, the continuity of the induced current path plays a vital role in EMI shielding performance. When the electric field of

the incident EM wave ran parallel to the carbon fiber direction (0°), the vertical slit blocked the current path of the CFRP and caused greater obstruction and discontinuity for the induced current than the parallel slit, as shown in Fig. 4.7(a). All of this caused the significant decrease in SE values with the existence of slits in the CFRP composites, with the vertical slit leading to more EM leakage, resulted in the lower SE values, as shown in Fig. 4.7(b). Thus, it can be concluded that both the slit and the slit orientation can be identified successfully at a 0° incident angle.

When the incident angles were 45° and 90°, an interesting result emerged in that the EMI SE values of the vertical-slit CFRP were higher than with the parallel-slit CFRP, as shown in Fig. 4.7(c) and Fig. 4.7(d), which was the opposite to the result at the 0° incident angle. This was because the incident angle between the slit and the electric field direction determined the EMI shielding performance of the CFRP. Taking the 90° incident angle as an example, the parallel-slit CFRP, in which the slit was perpendicular to the electric field of the EM waves, led to greater discontinuity of the incident current, which resulted in a lower SE value. In addition, the SE value difference between the vertical-slit CFRP and the parallel-slit CFRP at the 0° test angle was larger than that at the 90° incident angle, as shown in Fig. 4.7(b) and Fig. 4.7(d). It can be concluded that the EMW-NDT method could be applied to identify the slit orientation on the CFRP composites, while the attention must be paid to the evaluation criteria when using various incident angles.

4.3.5 Detection sensitivity of slit length by ΔS_{21} (dB)

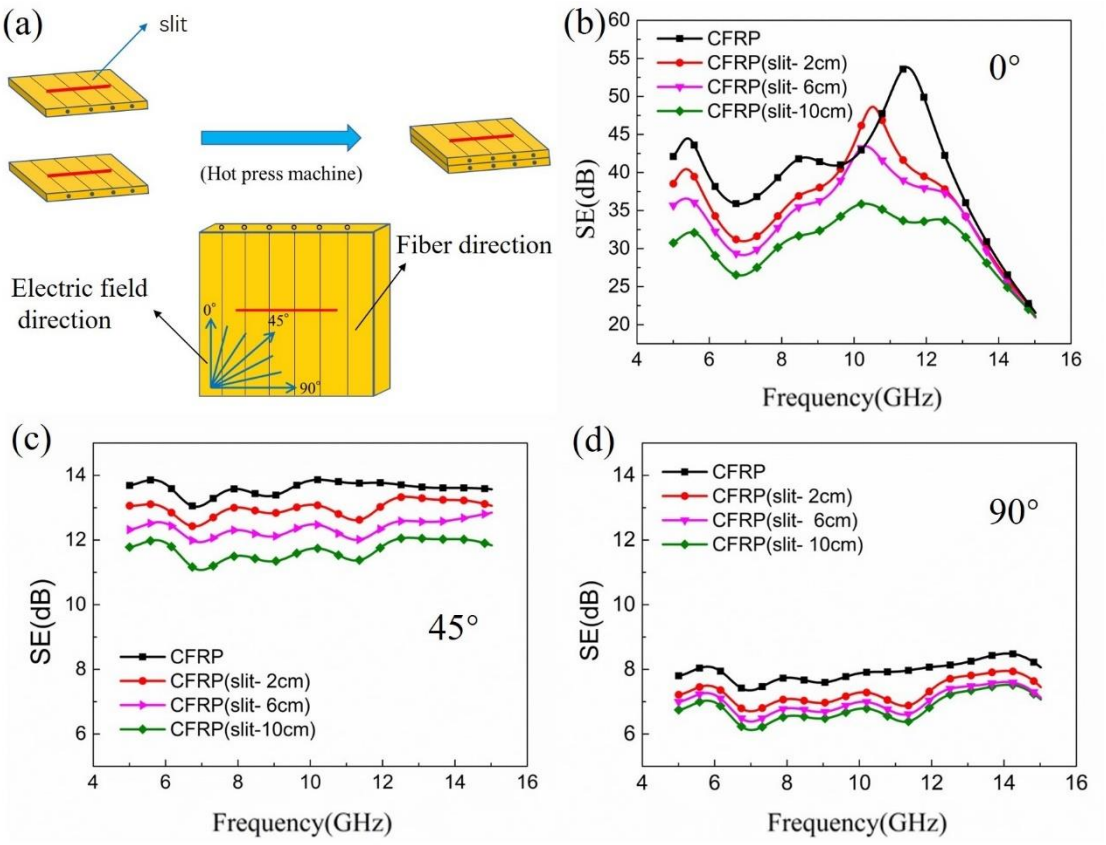

Fig. 4.8. (a) CFRP with slit; SE values of CFRP at different testing angles of (b) 0°, (c) 45°, and (d) 90°

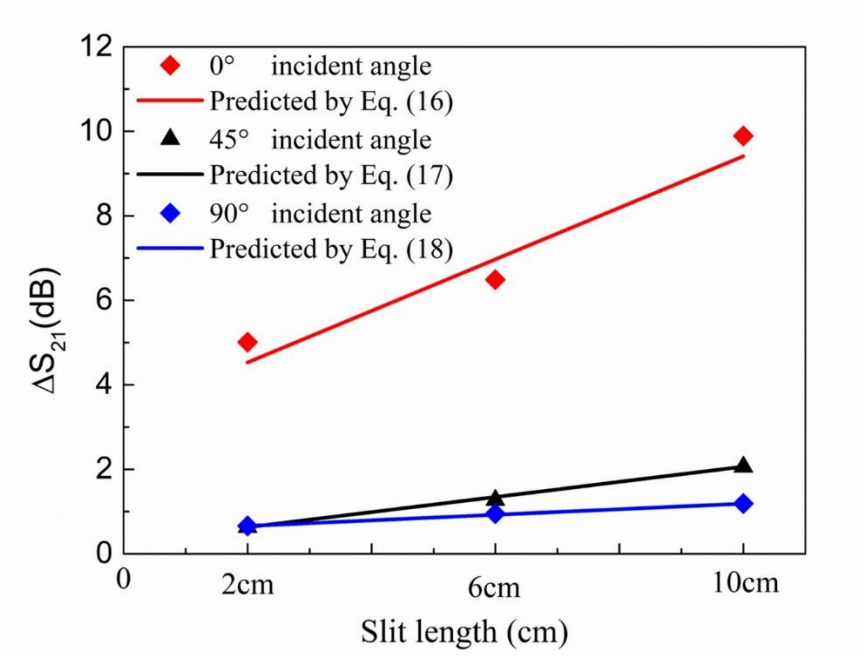

Fig. 4.9 Detection sensitivity of slit length at different incident angles under 8 GHz

The influence of the slit length in the vertical-slit type was investigated. Here, vertical slits with various lengths (2, 6 and 10 cm) were introduced in the unidirectional CFRP, with the width of the slits around 0.1 mm, as shown in Fig. 4.8 (a). As Fig. 4.8 (b) shows, a clear difference in SE value with the slit length change was observed at the 0° incident angle, with strong peaks appearing at 10.2 GHz. Meanwhile, the best detection sensitivity appeared at the 0° incident angle under 8 GHz as shown in Fig. 4.9. For the 45° and 90° incident angles, although their detection sensitivity was lower than that of the 0° incident angle (Fig. 4.8 (c), (d)), it was sufficient to determine the slit length of CFRP composite by the detection sensitivity. The results show that the detection sensitivity value increased almost linearly with the increment of the slit length (d), which can be expressed approximately by the linear equation as follows:

ΔS_{21} (dB)=0.611×d+3.79 for the 0° incident angle (16)

ΔS_{21} (dB)=0.179×d+0.272 for the 45° incident angle (17)

ΔS_{21} (dB)=0.066×d+0.528 for the 90° incident angle (18)

As shown in Fig. 4.9, the predicted detection sensitivity values by the above equations are in good consistent with the experimental result, that means the slit length could be predicted by the proposed formulas.

4.4 Conclusions

Based on the EMI shielding performance of CFRP composites, a novel NDT method (EMW-NDT) for assessing the damage in CFRP composites was presented in this chapter. The detection capacity of the EMW-NDT method in relation to the

delamination and crack damage was investigated and identified systematically. Besides, the effect of the incident angle of the EM wave on the detection sensitivity for CFRPs was also comprehensively discussed. The results indicated that delamination damage with different sizes and thicknesses could be identified with high detection sensitivity using the proposed method. Then, a reasonable detection sensitivity in the damage volume change of delamination was confirmed, with the damage aera ratio of 12.6%/dB and a thickness change of 5.6 dB/mm. In terms of crack damage, both the slit and its length were detected, with the slit direction also identified successfully based on the characteristics of EMI shielding anisotropy in CFRPs. The result also shows that the incident angle of the EM wave plays a vital role in detection sensitivity due to the skin effect. The EMW-NDT method is based on the electromagnetic wave technique and is contactless, which means a coupling medium is not required in the detection process. It is proved that the proposed method can be applied to the damage detection of CFRP composites, which is both rapid and efficient. As such, the proposed EMW-NDT method exhibits vast potential for NDT application of CFRP composites and uses in various fields.

Reference

[1] H.A. Maples, O. Smith, C. Burgstaller, P. Robinson, A. Bismarck, Improving the ply/interleaf interface in carbon fibre reinforced composites with variable stiffness. Composites Science and Technology, 128 (2016) 185-192.

[2] Y.F. Zhu, L. Zhang, T. Natsuki, Y.Q. Fu, Q.Q. Ni, Facile synthesis of BaTiO3 nanotubes and their microwave absorption properties. ACS Appl Mater Interfaces, 4 (2012) 2101-2106.

[3] T. Bergmann, S. Heimbs, M. Maier, Mechanical properties and energy absorption capability of woven fabric composites under ±45° off-axis tension. Composite Structures, 125 (2015) 362-373.

[4] Q.Q. Ni, Y.F. Zhu, L.J. Yu, Y.Q. Fu, One-dimensional carbon nanotube@barium titanate@polyaniline multiheterostructures for microwave absorbing application. Nanoscale Res Lett, 10 (2015) 174.

[5] C.-S. Zhang, Q.-Q. Ni, S.-Y. Fu, K. Kurashiki, Electromagnetic interference shielding effect of nanocomposites with carbon nanotube and shape memory polymer. Composites Science and Technology, 67 (2007) 2973-2980.

[6] L. Cheng, G.Y. Tian, Comparison of Nondestructive Testing Methods on Detection of Delaminations in Composites. Journal of Sensors, 2012 (2012) 1-7.

[7] B. Salski, W. Gwarek, P. Korpas, S. Reszewicz, A.Y.B. Chong, P. Theodorakeas, I. Hatziioannidis, V. Kappatos, C. Selcuk, T.-H. Gan, M. Koui, M. Iwanowski, B. Zielinski, Non-destructive testing of carbon-fibre-reinforced polymer materials with a radio-frequency inductive sensor. Composite Structures, 122 (2015) 104-112.

[8] D.D.L. Chung, Processing-structure-property relationships of continuous carbon fiber polymer-matrix composites. Materials Science and Engineering: R: Reports, 113 (2017) 1-29.

[9] W. Gong, J. Chen, E.A. Patterson, Buckling and delamination growth behaviour of delaminated composite panels subject to four-point bending. Composite Structures, 138 (2016) 122-133.

[10] T. Yamane, A. Todoroki, Doublet analysis of changes in electric potential induced

by delamination cracks in carbon-fiber-reinforced polymer laminates. Composite Structures, 176 (2017) 217-224.

[11] J.C. Moulder, E. Uzal, J.H. Rose, Thickness and conductivity of metallic layers from eddy current measurements. Review of Scientific Instruments, 63 (1992) 3455-3465.

[12] Z. Li, Z. Meng, A Review of the Radio Frequency Non-destructive Testing for Carbon-fibre Composites. Measurement Science Review, 16 (2016) 68-76.

[13] D. Wu, F. Cheng, F. Yang, C. Huang, Non-destructive testing for carbon-fiber-reinforced plastic (CFRP) using a novel eddy current probe. Composites Part B: Engineering, 177 (2019) 107460.

[14] L.U. Daura, G. Tian, Q. Yi, A. Sophian, Wireless power transfer-based eddy current non-destructive testing using a flexible printed coil array. Philos Trans A Math Phys Eng Sci, 378 (2020) 20190579.

[15] K. Mizukami, A.S.b. Ibrahim, K. Ogi, N. Matvieieva, I. Kharabet, M. Schulze, H. Heuer, Enhancement of sensitivity to delamination in eddy current testing of carbon fiber composites by varying probe geometry. Composite Structures, 226 (2019) 111227.

[16] Y. He, G. Tian, M. Pan, D. Chen, Non-destructive testing of low-energy impact in CFRP laminates and interior defects in honeycomb sandwich using scanning pulsed eddy current. Composites Part B: Engineering, 59 (2014) 196-203.

[17] K. Mizukami, Y. Mizutani, A. Todoroki, Y. Suzuki, Analytical solutions to eddy current in carbon fiber-reinforced composites induced by line current. Advanced Composite Materials, 25 (2015) 385-401.

[18] S. Jiao, J. Li, F. Du, L. Sun, Z. Zeng, Characteristics of Eddy Current Distribution in Carbon Fiber Reinforced Polymer. Journal of Sensors, 2016 (2016) 1-8.

[19] A.M. Amaro, P.N.B. Reis, M.F.S.F. de Moura, J.B. Santos, Damage detection on laminated composite materials using several NDT techniques. Insight - Non-Destructive Testing and Condition Monitoring, 54 (2012) 14-20.

[20] Q. Shen, M. Omar, S. Dongri, Ultrasonic NDE Techniques for Impact Damage Inspection on CFRP Laminates. Journal of Materials Science Research, 1 (2011).

[21] A.M. Amaro, J.B. Santos, J.S. Cirne, Delamination Depth in Composites Laminates With Interface Elements and Ultrasound Analysis. Strain, 47 (2011) 138-145.

[22] M. Kersemans, A. Martens, K. Van Den Abeele, J. Degrieck, F. Zastavnik, L. Pyl, H. Sol, W. Van Paepegem, Detection and Localization of Delaminations in Thin Carbon Fiber Reinforced Composites with the Ultrasonic Polar Scan. Journal of Nondestructive Evaluation, 33 (2014) 522-534.

[23] M. Kusano, H. Hatano, M. Watanabe, S. Takekawa, H. Yamawaki, K. Oguchi, M. Enoki, Mid-infrared pulsed laser ultrasonic testing for carbon fiber reinforced plastics. Ultrasonics, 84 (2018) 310-318.

[24] Jan-Carl Grager, Daniel Kotschate, Jakob Gamper, Mate Gaal, Katja Pinkert, Hubert Mooshofer, Matthias Goldammer, C.U. Grosse, in: 12th European conference on Non-Destructive Testing, Gothenburg, Sweden, 2018.

[25] Y.Y.Hung, Applications of digital shearography for testing of composite structures. Composites Part B: Engineering, 30 (1999) 765-733.

[26] V. Pagliarulo, V. Lopresto, A. Langella, V. Antonucci, M.R. Ricciardi, P. Ferraro, Non-destructive evaluation of impact damage on carbon fiber laminates: Comparison between ESPI and Shearography. 1740 (2016) 040002.

[27] C. Goidescu, H. Welemane, C. Garnier, M. Fazzini, R. Brault, E. Péronnet, S. Mistou, Damage investigation in CFRP composites using full-field measurement techniques: Combination of digital image stereo-correlation, infrared thermography and X-ray tomography. Composites Part B: Engineering, 48 (2013) 95-105.

[28] Mathieu Tartare, Veronique Rebuffel, Nicolas Ducros, L. Verger, in: 11th European Conference on Non-Destructive Testing (ECNDT 2014), Prague, Czech Republic, 2014.

[29] S. Gholizadeh, A review of non-destructive testing methods of composite materials. Procedia Structural Integrity, 1 (2016) 50-57.

[30] C.Q. Wu, W.P. Wang, Q.G. Yuan, Y.J. Li, W. Zhang, X.D. Zhang, Infrared Thermography Non-Destructive Testing of Composite Materials. Advanced Materials Research, 291-294 (2011) 1307-1310.

[31] R. Sutthaweekul, G. Tian, Z. Wang, F. Ciampa, Microwave open-ended waveguide for detection and characterisation of FBHs in coated GFRP pipes. Composite Structures, 225 (2019) 111080.

[32] V.P. Vavilov, Modeling and characterizing impact damage in carbon fiber composites by thermal/infrared non-destructive testing. Composites Part B: Engineering, 61 (2014) 1-10.

[33] R. Steinberger, T. Valadasleitao, E. Ladstatter, G. Pinter, W. Billinger, R. Lang, Infrared thermographic techniques for non-destructive damage characterization of carbon fibre reinforced polymers during tensile fatigue testing. International Journal of Fatigue, 28 (2006) 1340-1347.

[34] C. Meola, S. Boccardi, G.M. Carlomagno, N.D. Boffa, E. Monaco, F. Ricci, Nondestructive evaluation of carbon fibre reinforced composites with infrared thermography and ultrasonics. Composite Structures, 134 (2015) 845-853.

[35] D.K. Ghodgaonkar, V.V. Varadan, V.K. Varadan, A free-space method for measurement of dielectric constants and loss tangents at microwave frequencies. IEEE Transactions on Instrumentation and Measurement, 38 (1989) 789-793.

[36] V.V. Varadan, R.D. Hollinger, D.K. Ghodgaonkar, V.K. Varadan, Free-space, broadband measurements of high-temperature, complex dielectric properties at microwave frequencies. IEEE Transactions on Instrumentation and Measurement, 40 (1991) 842-846.

[37] U.C. Hasar, Non-destructive testing of hardened cement specimens at microwave frequencies using a simple free-space method. NDT & E International, 42 (2009) 550-557.

[38] M. Ozturk, U.K. Sevim, O. Akgol, M. Karaaslan, E. Unal, An electromagnetic non-destructive approach to determine dispersion and orientation of fiber reinforced concretes. Measurement, 138 (2019) 356-367.

[39] R.H.Knibbs, J.B.Morris, The effects of fibre orientation on the physical properties of composites. Composites 5(1974) 209-218.

[40] A. Todoroki, Electric Current Analysis for Thick Laminated CFRP Composites.

Transactions of the Japan society for aeronautical and space sciences, 55 (2011) 237-243.
[41] Richard B. Schulz, V.C.Plantz, D.R.Brush, Electromagnetic shielding theory and practice. IEEE Transactions on electromagnetic compatibility, 30 (1988) 187-201.
[42] G.M. Kunkel, Shielding of Electromagnetic Waves Theory and Practice, Springer, Cham, Springer Nature Switzerland AG, 2020.

Chapter 5

Conclusions

5 Conclusions

Continuous carbon fiber reinforced polymers (CFRP) composites, particularly prepreg stacked composites, have anisotropic properties, including anisotropy of electrical conductivity and dielectric characteristics. The EMI shielding anisotropy was confirmed for the first time by the coaxial transmission line method, and the optimization of EMI shielding performance of CFRP by changing the composites' structure were also investigated systematically. In order to provide a theoretical analysis of EMI shielding anisotropy, a specially designed free-space measurement was set up in one direction vibration of incident EM wave, which can measure shielding performance of CFRP in any specified direction. Meanwhile, based on the good EMI shielding performance of CFRP composites, especially its shielding anisotropy, a novel NDT method using electromagnetic wave technique was proposed to detect defects of CFRP composites.

In Chapter 1, an overview of the EMI shielding materials, shielding mechanisms, and the EMI shielding measurements has been present. Meanwhile, the non-destructive testing of CFRP composites also has been reviewed.

In Chapter 2, the effect of the angle between the direction of fibers in anisotropic CFRP and the electric field on EMI shielding performance was investigated. The EMI shielding effectiveness of CFRP prepared with various types of carbon fibers, different numbers of laminate layers, and different fiber orientation were also determined. The

anisotropy of electromagnetic wave shielding was confirmed for the first time using the coaxial transmission line method. The CFRP (radial) composites provided the best shielding performance, its total SE was approximately 25.8 dB at 15 GHz, while the CFRP (0˚/0˚) shows the lowest SE (15.9 dB). This was attributed mainly to the quasi-radial distribution of the carbon fibers, which clearly aligned with the electrical field direction of the EM waves. The four-ply CFRP (0°/90°/0°/90°) with three cross-layers had the excellent shielding value of 28.9 dB at 15 GHz, that was far superior to that of a unidirectional CFRP (0°/0°/0°/0°) composite (SE= 18.6 dB), and it even outperformed an eight-ply unidirectional CFRP composite (SE= 22.6 dB). This meant that the (0°/90°/0°/90°) CFRP composite shielded against approximately 99.9% of the EM radiation. Laminated structures governed SE, and the number of cross-layers in the composites improved their EMI shielding performance.

In Chapter 3, the EMI shielding anisotropy of CFRP materials was discussed. The electrical conductivity of unidirectional CFRP composites varies due to the fiber orientation angles, and the calculated results from the formulas were consistent with the experiment values. All the characteristics mentioned above are key issues leading to the EMI shielding anisotropy of CFRP composites. The obvious EMI shielding anisotropy of unidirectional CFRP composites is clarified by the experimental results using specified set-up of free-space measurement. The theoretical formula can predict the EMI shielding value at different carbon fiber orientation angles, and the predicted results were highly consistent with the experimental results. A comparison of free-space measurement and coaxial transmission line method was also conducted, and the

influence of electric anisotropy on the test results was further discussed. With these results, the mechanism of EMI shielding anisotropy of CFRP composites is clarified, which will provide an effective design of EMI products with a designable shielding direction and frequency.

In Chapter 4, a new type of NDT method using electromagnetic wave technique was proposed. This NDT method is a non-contact measurement and does not require the couplants during testing. It was proven that the proposed EMW-NDT method is effective in detecting damages such as delamination, crack or other defects in CFRP composites. The EMW-NDT method's detection capacity to the delamination size, delamination thickness, and slits in CFRP composites was investigated. A reasonable sensitivity to the damage volume change in delamination was confirmed with a damage area ratio of 12.6%/dB and a thickness change of 5.5 dB/mm. The results confirmed that the proposed method demonstrates good detection sensitivity to delamination size and thickness. In terms of crack damage, the slit and its length were detected and the slit direction was successfully identified in this study based on the characteristics of the EMI shielding anisotropy in CFRPs. It is proved that the proposed NDT method can be applied to the damage detection of CFRP composites, which is both rapid and efficient.

In chapter 5, we summarized the EMI shielding anisotropy of CFRP composites, and convinced the reliability of the EMW-NDT method based on electromagnetic wave technology.

ACCOMPLISHMENTS

LIST OF PUBLICATION

❋❋❋❋❋❋❋❋❋❋❋❋❋❋❋❋❋❋❋❋❋❋❋❋❋❋❋❋❋❋❋❋❋❋❋❋❋

Journal Publications

1. Jun Hong, Ping Xu, Hong Xia, Zhenzhen Xu, Qing-Qing Ni. Electromagnetic interference shielding anisotropy enhanced by CFRP laminated structures, Composites Science and Technology 203 (2021) 108616

2. Qing-Qing Ni, Jun Hong, Ping Xu, Zhenzhen Xu, Kirill Khvostunkov, Hong Xia. Damage detection of CFRP composites by electromagnetic wave nondestructive testing (EMW-NDT), Composites Science and Technology 210 (2021) 108839

3. Jun Hong, Ping Xu. Electromagnetic interference shielding anisotropy of unidirectional CFRP composites, Materials 14(8) (2021) 1907

International Conference

1. Jun Hong, Qing-Qing Ni. Effect of Fiber Orientation on Electromagnetic Interference Shielding Effectiveness of CFRP Laminates, Symposium of advanced composites, Ueda, SAC2017 (October 2017, Ueda, Japan).

Domestic Conference

1. 洪鈞，夏紅，倪慶清. CFRPの電磁波遮蔽特性に及ぼすカーボ ン繊維配向の影響，2019年繊維学会秋季研究発表会，上田.

ACKNOWLEDGMENTS

First and foremost, I would like to express my sincere gratitude to my supervisor Prof. Qing-Qing Ni for providing me the opportunity to study in Shinshu University, and I also thankful for his support and guidance throughout my PhD period. Meanwhile, I like to express my gratitude to Dr. Hong Xia for her continuous guidance and support to my research work.

I thank Prof. Toshiaki Natsuki as my co-supervisor, for his extensive advises and guidance for this research work. Special thanks to all former and current members of Ni Lab (Dr. Hairong Cheng, Dr. Xiaoyu Guan, Dr. Chongchao Li, Dr. Wendan Yang, Mr. Zhe Yang, Mr. Yinan Jing) for their assistance and suggestions on my research.

I want to express my gratitude to Chinese Scholarship Committee for financial support.

I also thank to all my friends at Shinshu University, especially Dr. Zhong Wang, Dr. Bing Liu, Dr. Peng Zhu, for their assistance and help of experimental tests.

Special thanks to Prof. Songmei Bi and Prof. Zhenzhen Xu at Anhui Polytechnic University for their suggestions and warm encouragement, which have boosted my

research work.

Finally, I would like to thank my beloved families for their support, understanding and concern during my PhD period. I also want to thank all my friends at Shinshu University.